

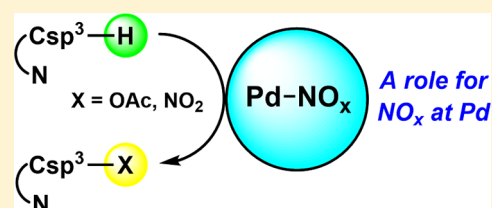
Redox Couple Involving NO_x in Aerobic Pd-Catalyzed Oxidation of $\text{sp}^3\text{-C-H}$ Bonds: Direct Evidence for $\text{Pd-NO}_3^-/\text{NO}_2^-$ Interactions Involved in Oxidation and Reductive Elimination

Margot N. Wenzel,[†] Philippa K. Owens,[‡] Joshua T. W. Bray,[§] Jason M. Lynam, Pedro M. Aguiar, Christopher Reed, James D. Lee, Jacqueline F. Hamilton, Adrian C. Whitwood, and Ian J. S. Fairlamb*[¶]

Department of Chemistry, University of York, York YO10 5DD, United Kingdom

S Supporting Information

ABSTRACT: NaNO_3 is used in oxidative Pd-catalyzed processes as a complementary co-catalyst to common oxidants, e.g., Cu^{II} salts, in C–H bond activation and Wacker oxidation processes. NaNO_3 and NaNO_2 (with air or O_2) assist the $\text{sp}^3\text{-C-H}$ bond acetoxylation of substrates bearing an N-directing group. It has been proposed previously that a redox couple is operative. The role played by NO_x anions is examined in this investigation. Evidence for an NO_x anion interaction at Pd^{II} is presented. Palladacyclic complexes containing NO_x anions are competent catalysts for acetoxylation of



8-methylquinoline, with and without exogenous NaNO_3 . The oxidation of 8-methylquinoline to the corresponding carboxylic acid has also been noted at Pd^{II} . ^{18}O -Labeling studies indicate that oxygen derived from nitrate appears in the acetoxylation product, the transfer of which can only occur by interaction of ^{18}O at Pd with a coordinating-acetate ligand. Nitrated organic intermediates are formed under catalytic conditions, which are converted to acetoxylation products, a process that occurs with (50°C) and without Pd (110°C). A catalytically competent palladacyclic dimer intermediate has been identified. Head-space analysis measurements show that NO and NO_2 gases are formed within minutes on heating catalytic mixtures to 110°C from room temperature. Measurements by in situ infrared spectroscopy show that N_2O is formed in $\text{sp}^3\text{-C-H}$ acetoxylation reactions at 80°C . Studies confirm that cyclopalladated NO_2 complexes are rapidly oxidized to the corresponding NO_3 adducts on exposure to $\text{NO}_2(\text{g})$. The investigation shows that NO_x anions act as participating ligands at Pd^{II} in aerobic $\text{sp}^3\text{-C-H}$ bond acetoxylation processes and are involved in redox processes.

INTRODUCTION

The catalytic and selective C–H bond functionalization of organic substrates is of fundamental importance in synthetic chemistry.¹ Significant effort has been directed toward solving the issue of challenging C–H bond functionalization reactions in a variety of substrates. While much has been accomplished in the field of selective $\text{C}(\text{sp}^2)\text{-H}$ functionalizations, reactions of less-activated $\text{C}(\text{sp}^3)\text{-H}$ bonds, e.g., as found in secondary and tertiary alkyls and allylic and benzylic systems, has proven more challenging. In driving the development of challenging $\text{C}(\text{sp}^3)\text{-H}$ bond functionalization processes, mechanistic studies (both experimental and computational) are essential—the key role played by a particular metal, ligand (neutral or anionic), additive, or specific substrate class, under an eclectic array of reaction conditions, cannot be overstated. These points are evidenced from a series of recent studies exploiting the redox activity of nitrate (NO_3^-) and/or nitrite (NO_2^-) anions, *vide infra*. In C–H bond functionalization chemistry, the role of such anions at Pd is poorly defined, requiring mechanistic examination, particularly if the catalytic behavior of reaction processes utilizing these anions is to be fully realized. Of particular note is the work of Stahl and co-workers, who reported selective benzene acetoxylation using NO_x -based redox mediators at Pd.²

Sanford and co-workers³ reported a remarkable methodology for the acetoxylation of unactivated $\text{C}(\text{sp}^3)\text{-H}$ bonds, i.e., in oxime ether and pyridine-type derivatives, with the nitrogen atom playing the role of directing group to Pd. The reactions utilized $\text{Pd}(\text{OAc})_2$ as a catalyst and dioxygen as the terminal oxidant in acetic acid (AcOH)/acetic anhydride (Ac_2O) (Figure 1). Vedernikov and co-workers reported a similar oxidative catalyst process using Pd^{II} –pyridinecarboxylic acid systems.⁴

Addition of NaNO_3 —proposed to be a redox co-catalyst³—was important for effective catalysis (NO was detected, formed by decomposition of NaNO_3 , and it is of note that NaNO_2 can play a similar activating role). Using ^{18}O -labeled dioxygen, it was deduced that oxygen incorporation into the acetoxylation product derives from acetic acid (solvent) and not O_2 . A key question that we asked was if NO_3^- and/or NO_2^- are critical ligands (pseudohalides) at Pd within the catalytic cycle? If $\text{Pd-NO}_3/\text{Pd-NO}_2$ species are present, then C–O bond formation ought to be favored over C–N bond formation as acetoxylation products are the only ones observed, despite reductive elimination of NO_2 being feasible at Pd.

Received: October 20, 2016

Published: January 11, 2017

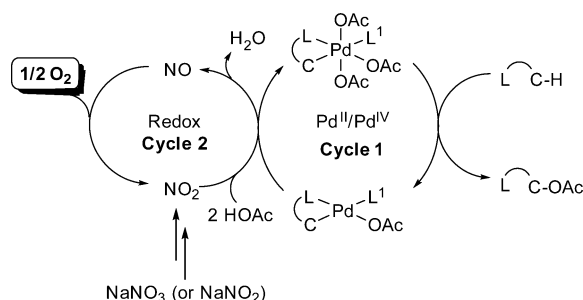


Figure 1. Proposed mechanism for C(sp³)-H bond functionalization³ using a NO_x redox-couple at Pd.

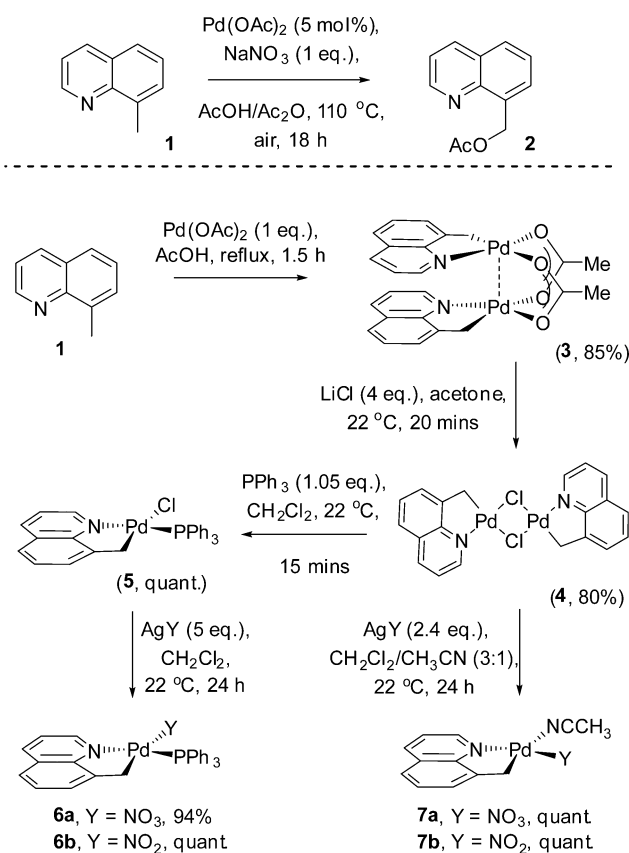
Examining the role played by NO₃⁻/NO₂⁻ anions is arguably essential for the development of other redox-coupled Pd catalysis, particularly as nitrite (AgNO₂) has been shown to be directly involved in a recently developed catalyst-controlled Wacker oxidation.⁵ Grubbs and Stoltz further reported Pd-catalyzed aerobic intramolecular aminoacetoxylation of alkenes enabled by Cu(NO₃)₂, the latter acting as an electron-transfer mediator.⁶ Also, Xu and co-workers demonstrated that MnO₃ (M = K or Ag) can act as a co-catalyst in C-H bond fluorination chemistry.⁷ Xu proposed the involvement of Pd^{II}/Pd^{IV} species based on ESI-MS analysis of the catalytic reaction under working conditions. Moreover, they suggested [Pd(NO₃)]⁺ as the active catalyst species, although direct evidence for its existence was not presented. These recent findings are underpinned by a series of long-standing studies on other catalytic processes involving nitrate/nitrite anions at Pd^{II}. For example, formation of ethylene glycol monoacetate from ethylene in acetic acid solution containing LiNO₃ and Pd(OAc)₂ is accompanied by oxygen atom transfer from the oxidant to the carbonyl group of the product (confirmed by ¹⁷O-labeling).⁸ Henry reported that NaNO₃ and NaNO₂ can be used as oxidants in the C(sp²)-H oxidation of various aromatics, where the nitrate/nitrite can play a role similar to that of Cu.⁹ In the 1980s, several groups explored the catalytic properties of [Pd(Cl)(NO₂)(CH₃CN)] in the oxidation of olefins to either epoxides and ketones, as well as glycol monoacetate.^{10–14} Bäckvall and Heumann proposed that the nitrite ligand can be an active ligand at Pd^{II}, where the oxygen from PdNO₂ is transferred to the acetoxyated organic product.¹⁵

The dynamic behavior of nitrite at Pd^{II} has been of particular interest to our group¹⁶ and the group of Raithby,¹⁷ i.e., Pd-NO₂ and Pd-ONO linkage isomerization in various palladium complexes. Indeed, in expanding the scope of our work to understand the intimate role played by nitrite and nitrate at Pd^{II} and higher oxidation state Pd species, in addition to the role played by such anions in other catalytic Pd chemistry, we were attracted by the underlying role played by NO_x anions in Sanford's C(sp³)-H bond acetoxylation mediated by Pd^{II}/NaNO₃,³ in addition to the broader context of the work reported by Grubbs et al.^{5,6} Herein, we describe our mechanistic findings on the role played by NaNO₃ and Pd-NO₂/Pd-NO₃ species in the acetoxylation of C(sp³)-H bonds.

RESULTS

We directed our mechanistic studies to 8-methylquinoline (**1**). Under the conditions described by Sanford and co-workers (5 mol % Pd(OAc)₂, 1 equiv of NaNO₃, AcOH/Ac₂O, air, 110 °C,

Scheme 1. Synthesis of Pd-NO₃/Pd-NO₂ Complexes



18 h), the acetoxyated product (**2**) was formed in 80% yield (Scheme 1).³ The Pd(OAc)₂ used throughout this study is Pd₃(OAc)₆ (verified by IR and NMR; stated as >99% purity by the supplier).¹⁸ In our hands, we recorded >99% conversion to **2** by both GC and ¹H NMR spectroscopic analysis of the crude reaction, validating it as a starting point for further study.

The overwhelming evidence from the field is that the first committed step in the catalytic cycle involves C-Pd bond formation by C-H bond functionalization (cyclopalladation),¹⁹ likely by a concerted metalation deprotonation (CMD) reaction.²⁰ Stoichiometric reaction of Pd(OAc)₂ with **1** (1:1) in AcOH at reflux for 1.5 h gave the dinuclear Pd^{II} complex (**3**) in 85% yield (Scheme 1).

A single crystal of **3** was grown from CH₂Cl₂/pentane and found to be suitable for X-ray diffraction study, confirming the structure of the cyclopalladated system as a mixture of *syn/anti* isomers (Figure 2), which is consistent with the other characterization data. A prominent feature of the X-ray structure is the slipped π -stacking between quinolinyl groups, which occurs in both *syn/anti* isomers. A palladophilic interaction [dashed line between Pd(1) and Pd(2)] is indicated as the bond distance is within the sum of the van der Waals radii for the two Pd centers. The introduction of both NO₃⁻/NO₂⁻ anions to the Pd^{II} centers could be achieved starting from the Cl-bridged dinuclear Pd^{II} complex **4** (synthesized in 80% yield by treatment of **3** with LiCl). The mononuclear Pd^{II} complex **5** was formed quantitatively on treatment of **4** with a slight excess of PPh₃. Pd-NO₃ (**6a**) and Pd-NO₂ (**6b**) mononuclear complexes could be synthesized from **5** by treatment with AgNO₃ and AgNO₂, respectively.

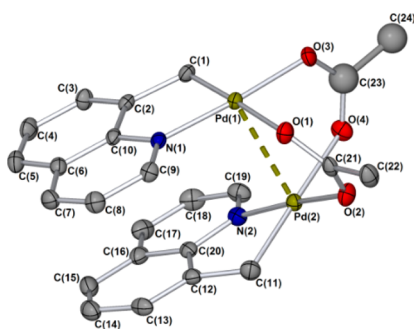


Figure 2. X-ray structure of **3**. Note that the structure is disordered over two positions (only the *anti*-isomer shown here); the C(23) and C(24) atoms are not resolved enough to be displayed as thermal ellipsoids. Selected bond distances (Å) and angles (deg): Pd1...Pd2 = 2.8408(4), O1–Pd1 = 2.176(3), O2–Pd2 = 2.042(3), O3–Pd1 = 2.058(3), O4–Pd2 = 2.172(4), N1–Pd1 = 2.010(2), N2–Pd2 = 2.005(3), C1–Pd1 = 1.996(3), C11–Pd2 = 2.003(3); C1–Pd1–N1 = 83.96(11), C11–Pd2–N2 = 83.68(12), N2–Pd2–O2 = 173.56(11), N1–Pd1–O3 = 174.82(11).

Complex **6a** was crystallized from CH₂Cl₂/cyclohexene, and its structure was confirmed by single-crystal X-ray diffraction (Figure 3). The NO₃ ligand is found to be *trans* to the sp³-

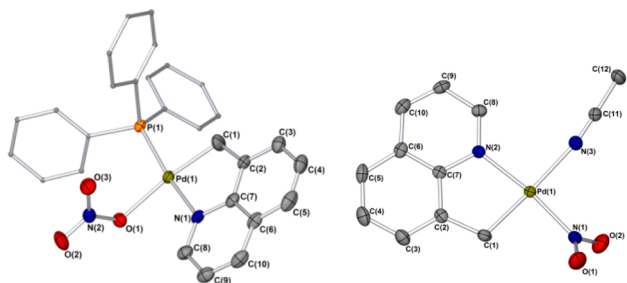


Figure 3. X-ray structures of **6a** (left) and **7b** (right). Selected bond distances (Å) and angles (deg) for **6a**: C1–Pd1 = 1.9900(18), N1–Pd1 = 2.0818(14), O1–Pd1 = 2.1250(13), N2–O1 = 1.289(2), N2–O2 = 1.240(2), N2–O3 = 1.232(2), P1–Pd1 = 2.2725(4); C1–Pd1–N1 = 81.61(6), C1–Pd1–O1 = 171.11(6), N1–Pd1–P1 = 175.42(4), O1–Pd1–P1 = 92.66(4). Selected bond distances (Å) and angles (deg) for **7b**: C1–Pd1 = 2.009(2), N1–O1 = 1.237(3), N1–O2 = 1.237(3), N1–Pd1 = 2.006(2), N2–Pd1 = 2.0355(19), N3–Pd1 = 2.1185(19); C1–Pd1–N2 = 83.67(8), C1–Pd1–N3 = 177.09(8), N1–Pd1–N2 = 172.26(7).

carbon center and *cis* to phosphorus and nitrogen (quinolinyl). The Pd–ONO₂ bond distance of Å = 2.125(13) is similar to that of related complexes.²¹ In addition, the CH₃CN adducts **7a** and **7b** could be synthesized quantitatively from **4**, which were fully characterized. The X-ray structure of **7b** is shown in Figure 3, which shows that the NO₂ ligand is *trans* to nitrogen (quinolinyl). The Pd–NO₂ bond distance, 2.006(2) Å, is similar to that of related Pd complexes reported by our group¹³ and others.²²

It did not prove possible to obtain single crystals of either **7a** or **6b** for X-ray crystallography studies. DFT calculations therefore allowed us to assess the single-point energies of the possible isomeric structures (see the Supporting Information for details). The *trans*-configuration is preferred in complex **7a** ($\Delta G_{cis-trans} = +13 \text{ kJ mol}^{-1}$). For complex **7b**, *cis*- and *trans*-isomeric forms can possess either *N*-bound or *O*-bound nitrite ligands, giving four isomeric possibilities. Both *cis*- and *trans*-

isomers containing an *O*-bound nitrite ligand are found to be ca. 21–29 kJ mol⁻¹ higher in energy than those containing *N*-bound nitrite ligands. In the latter case, however, the *cis*-[Pd(NO₂)(CAN)CH₃CN] complex is found to be of lower energy than *trans*-[Pd(NO₂)(CAN)CH₃CN] by 9 kJ mol⁻¹. Reductive elimination of the nitrated ligand backbone, which requires a *cis*-configuration, is feasible from this *cis*-Pd complex vide infra.

Taken together, the X-ray structures of **6a** and **7b** and the spectroscopic data for **6b** and **7a** indicate that nitrite and nitrate ligands can coordinate to a Pd^{II} center containing a cyclopalladated 8-methylenylquinoline.

Aerobic Oxidation of 8-Methylquinoline (1). The reference complexes gathered in Scheme 1, along with the benchmark catalyst Pd(OAc)₂, were evaluated in the aerobic oxidation of **1** to give **2** (Figure 4). For Pd(OAc)₂, there was

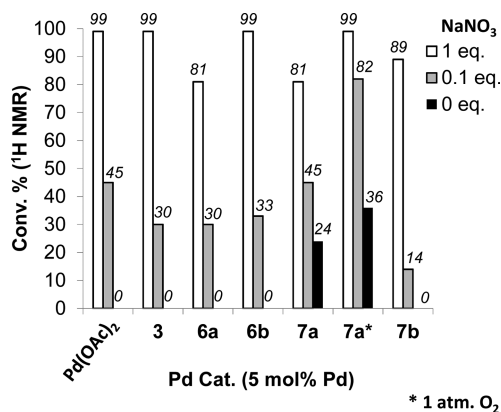


Figure 4. Catalytic activity of Pd complexes **3**, **6a**, **6b**, **7a**, and **7b** compared against Pd(OAc)₂ (5 mol %) with varying equivalents of NaNO₃ in the aerobic oxidation of **1** to give **2** (conditions: AcOH/Ac₂O, 110 °C, air, as for Scheme 1; conversion percentage relates to **2**).

>99% conversion using 1 equiv of NaNO₃. The % conversion dropped to 45% when 0.1 equiv of NaNO₃ was used, and negligible conversion was noted in its absence. The dinuclear Pd^{II} complex (**3**) is a catalytically competent species, showing a relatively similar profile to Pd(OAc)₂. The PPh₃-containing complexes **6a** and **6b** are also viable catalysts, with **6b** being more active under conditions using 1 equiv of NaNO₃. Complexes **3**, **6a**, and **6b** are not catalytically competent in the absence of NaNO₃. The stand-out result from Figure 4 is the catalyst efficacy of complex **7a**, which gave product **2** with 24% conversion (ca. 5 catalytic turnovers) in the absence of NaNO₃ and air as the oxidant. The reaction mediated by **7a** was found to be more effective under 1 atm of O₂, leading to a 36% conversion to **2** (ca. 7 catalytic turnovers). The effect of nitrate at Pd^{II} is therefore confirmed by this observation. The reason for the lack of activity of **6a** and **6b** is likely due to the phosphine ligand altering the kinetics of the catalytic process, particularly comparing directly **6a** with **7a** (CH₃CN being more labile than PPh₃).²³ Complex **7b**, containing the nitrite ligand, was inactive without NaNO₃.

A further series of reactions (**1** → **2**) were conducted using **7a** as the catalyst with varying equivalents of NaNO₃ under an atmosphere of either air or O₂ (Figure 5; for completeness, selected data from Figure 4 are included to reveal the essential trends). From these data, complex **7a** is found to be a viable catalyst, especially when lower equivalents of NaNO₃ are used.

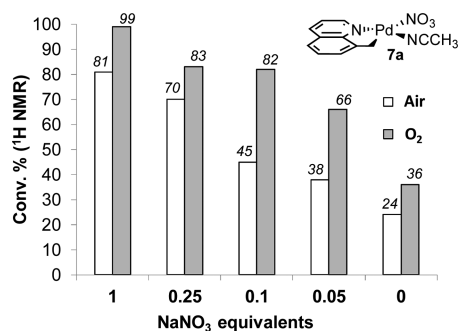


Figure 5. Catalytic activity of Pd complex **7a**, with varying equivalents of NaNO₃ in the presence of either air or O₂ in the aerobic oxidation of **1** to give **2** (other conditions as for Figure 4).

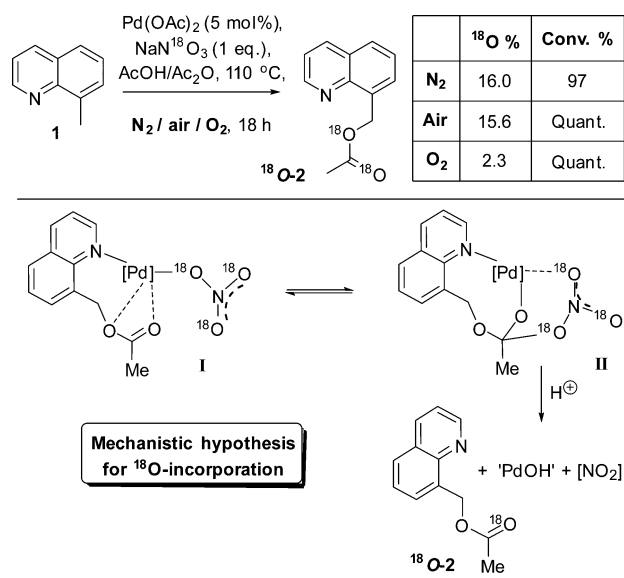
Finally, the effect of the nitrate equivalents on **7a** revealed that the relative drop in % conversion to **2** was more pronounced under air, whereas an absolute drop is evidenced under O₂ (1 atm). Good % conversions were observed between 0.05 and 0.1 equiv of NaNO₃.

It is worth noting that ceric ammonium nitrate (CAN; [(NH₄)₂Ce(NO₃)₆]) can be used as a co-catalyst in place of NaNO₃. CAN is known to generate NO₃[•] radicals, which are powerful one-electron oxidants.²⁴ The reaction of **1** → **2** mediated by Pd(OAc)₂ (5 mol %), AcOH/Ac₂O (7:1), 110 °C, 24 h and air, in the presence of 0.25 equiv of CAN, gave **2** in 95% yield.

Na¹⁸O₃-Labeling Experiments. The reaction of **1** → **2** mediated by Pd(OAc)₂ (5 mol %) was conducted using 1 equiv of NaN¹⁸O₃ (77.9% ¹⁸O-enriched) in AcOH/Ac₂O at 110 °C for 24 h under either N₂, air or O₂. Reactions were essentially quantitative (by GC analysis). For the reaction under N₂ (rigorous exclusion of air and degassing using Schlenk technique), the presence of 1 equiv of NaN¹⁸O₃ efficiently promotes the oxidative process, with 16% ¹⁸O incorporation (determined by MS) observed in product **2**. A similar outcome was recorded for the reaction conducted under air (15.6% ¹⁸O incorporation; note with a vast excess of AcOH/Ac₂O present, if free ¹⁸O exchange occurred in solution then the % incorporation would be negligible). In the case of the reaction under an O₂ atmosphere, negligible ¹⁸O incorporation into **2** was recorded. The results suggest that there is an exchange process occurring; i.e., the ¹⁸O label is washed out of NaN¹⁸O₃ in the reaction conducted under O₂ (i.e., into AcOH/Ac₂O).²⁵ Under N₂ or air the exchange process is diminished, leading to some ¹⁸O localization into acetoxylation product **2**. The outcome confirms that ¹⁸O is transferred from NO₃⁻ to Pd to product **2**, confirming its role as an active spectator ligand (note: we have not been able to determine whether the remaining ¹⁸O has been transferred to AcOH/Ac₂O under the catalytic conditions). One potential pathway showing intramolecular ¹⁸O-transfer is given in Scheme 2; the formation of Pd–O or Pd–OH species may explain the washing out of the ¹⁸O label from NaN¹⁸O₃ in the presence of pure O₂. In Sanford's study,³ ¹⁸O derived from ¹⁸O₂ (with unlabeled NaNO₃) was transferred into a different acetoxylation product to a small extent (5% ¹⁸O incorporation). Taken together with our results, this confirms that O₂, AcOH/Ac₂O and NaNO₃ are intimately connected through exchange processes.

On the Involvement of Higher Oxidation State Pd Species. Higher oxidation state Pd intermediates have been isolated and characterized in related aerobic acetoxylation

Scheme 2. Incorporation of ¹⁸O into Acetoxylation Product Using NaN¹⁸O₃ under Different Conditions (N₂/air/O₂)^a

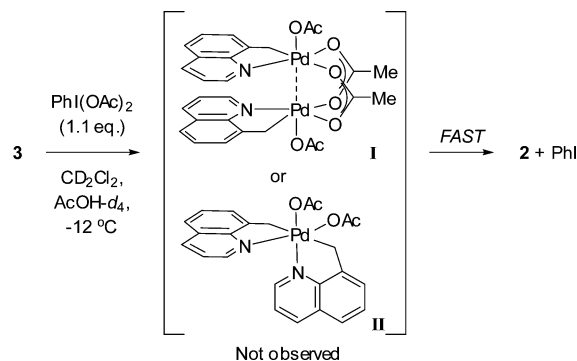


^aMechanism shows one pathway for ¹⁸O incorporation.

processes.²⁶ The incentive for this part of the investigation was to assess whether Pd^{III} or Pd^{IV} species could be detected in reactions involving a redox couple and nitrate. As PhI(OAc)₂ is a known powerful oxidant in Pd chemistry, we anticipated that it was useful to assess whether higher oxidation state Pd species formed from it were comparable with the Pd–NO_x chemistry.

Using standard acetoxylation conditions, the nitrate oxidant reacts with the in situ generated palladacycle. Having previously confirmed palladacycle **3** as catalytically competent,²⁷ we envisaged that higher oxidation state Pd species, i.e., Pd^{III} dinuclear or Pd^{IV} mononuclear complexes as depicted in Scheme 3, could be formed by reaction with typical oxidants.²⁶

Scheme 3. Reaction of PhI(OAc)₂ with Palladacycle 3



The reaction of palladacycle **3** with PhI(OAc)₂ in AcOH at –12 °C (note: at a substantially lower reaction temperature than the reported catalyzed process³) was monitored by ¹H NMR spectroscopy (700 MHz). The consumption of **3** was noted over ca. 1.5–2 h with the appearance of acetoxylation product **2** and PhI, but no other Pd intermediates were recorded (see the Supporting Information for NMR spectra).

A stoichiometric reaction of **3** with NaNO₃ was conducted under air at 50 °C in AcOH-*d*₄. In comparison with the PhI(OAc)₂ reaction conducted at –12 °C, detailed above, a higher temperature was deemed necessary for this stoichiometric

metric reaction to (1) aid solubility of NaNO_3 in AcOH and (2) mirror the working catalytic reaction conditions more closely (without excess **1** to slow down overall catalytic flux²⁷). The time course of the reaction was monitored by ^1H NMR spectroscopic analysis (see stacked ^1H NMR spectra in Figure 6). For comparison, reference spectra for substrate **1**, product

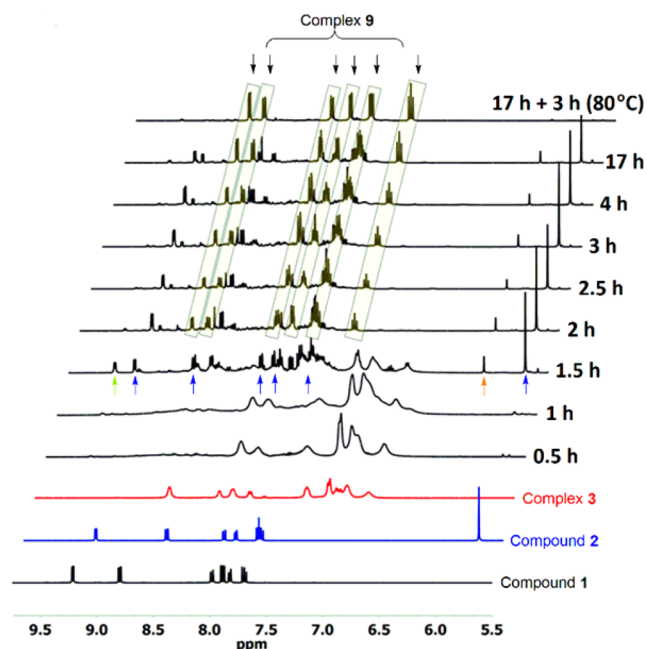


Figure 6. Reaction of **3** with NaNO_3 (1 equiv) in $\text{AcOH-}d_4$ at 50°C monitored by ^1H NMR spectroscopy (400 MHz). The ^1H NMR spectra for reference compounds **1–3** are given.

2, and complex **3** are included. Within 0.5 h of reaction, the proton signals belonging to **3** began to broaden, forming other species which are ill-defined on the NMR time scale. New products were formed after 1.5 h. One of these appears to correspond to **2** (identified by blue arrows) *vide infra*. Another organic product is formed as indicated by a singlet at ca. δ 6.20 ppm (highlighted by an orange arrow; see the following for confirmation of the structure). Other proton signals are observed, the most prominent being that at $\sim\delta$ 9.4 ppm (highlighted by a green arrow) the complete structure of which could not be discerned. After 2 h, a new product (which is **9**) appears, possessing six correlated proton environments (highlighted by yellow inset boxes).

Stopping the reaction at 4 h and crystallization gave two sets of single crystals which were found to be suitable for X-ray diffraction study. The first crystal recorded was found to be *trans*- $\text{Pd}(\text{OAc})_2(2)_2$, complex **8** (Figure 7). This indicates that the species observed by ^1H NMR (highlighted by blue arrows) is more likely *trans*- $\text{Pd}(\text{OAc})_2(2)_2$ (**8**) rather than **2** (confirmed by an authentic ^1H NMR spectrum of **8**). The second crystal was determined to be palladacycle **9**, where the ligand backbone had been fully oxidized to a carboxylate under the conditions of the reaction (Figure 8; see below for further crystallographic analysis). After 4 h (Figure 6), only one dominant species remains, which is palladacycle **9**.

The X-ray structure for palladacycle **9** is found in the *P*-1 space group ($Z = 2$). There is evidence of a $\text{Pd}^{\text{II}}\cdots\text{Pd}^{\text{II}}$ interaction; the Pd1-Pd2 distance is $2.7977(2)$ Å, which is shorter than the Pd1-Pd2 distance in palladacycle **3**

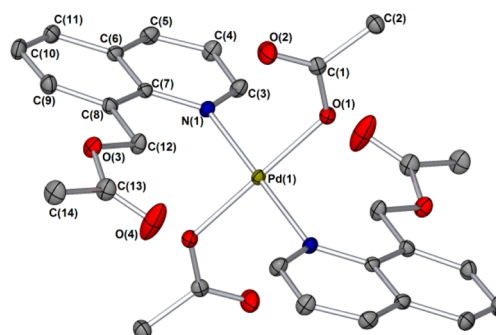


Figure 7. X-ray structure of *trans*- $\text{Pd}(\text{OAc})_2(2)_2$ (**8**). Selected bond distances (Å) and angles (deg) for **8**: $\text{N1-Pd1} = 2.0404(14)$, $\text{O1-Pd1} = 2.0064(13)$; $\text{O1-Pd1-N1} = 88.24(5)$, $\text{O1}^{(-X,-Y,1-Z)}\text{-Pd1-N1} = 91.76(5)$, $\text{N1-Pd1-N1}^{(-X,-Y,1-Z)} = 180.0$.

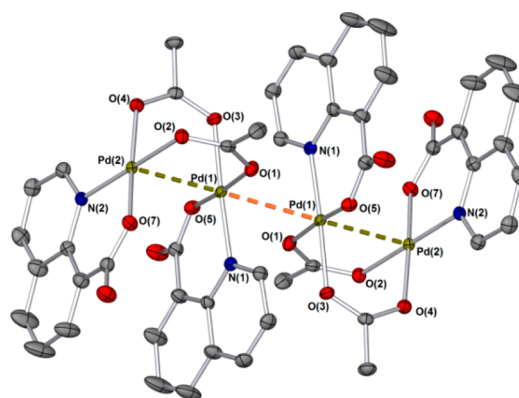
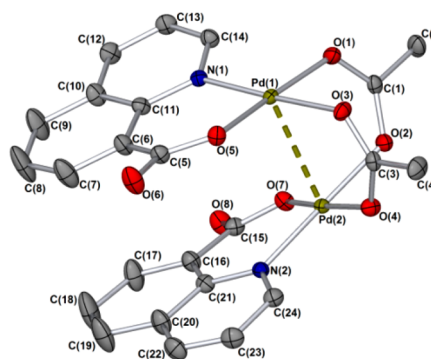


Figure 8. X-ray structure of **9** (top, single molecule; bottom, showing the packing between molecules and $\text{Pd1-Pd1}^{(2-X,1-Y,-Z)}$ interaction). Note that all hydrogens and three molecules of co-crystallized acetic acid are omitted from this drawing. Selected bond distances (Å) and angles (deg) for **9**: $\text{Pd2}\cdots\text{Pd1} = 2.7977(2)$, $\text{Pd1-N1} = 1.9931(16)$, $\text{Pd2-N2} = 1.9868(17)$, $\text{Pd1-O3} = 2.0210(13)$, $\text{Pd2-O2} = 2.0189(15)$; $\text{Pd1-O5} = 1.9538(15)$, $\text{Pd2-O7} = 1.9455(13)$; $\text{N1-Pd1-Pd2} = 102.60(4)$, $\text{N2-Pd2-Pd1} = 100.53(5)$, $\text{N1-Pd1-O3} = 177.04(5)$, $\text{N2-Pd2-O2} = 178.17(6)$.

($2.8408(4)$ Å). In addition, it is pertinent to mention the packing between molecules, which shows that $\text{Pd1-Pd1}^{(2-X,1-Y,-Z)}$ is separated by $3.0755(3)$ Å and $\text{Pd2-Pd2}^{(1-X,1-Y,-Z)}$ by $3.0631(3)$ Å.

A preparative-scale reaction of **3** with NaNO_3 was conducted, which gave **9** in quantitative yield (Figure 9). Palladacycle **9** was also accessed by reaction of 8-quinolinecarboxylic acid **10** with $\text{Pd}(\text{OAc})_2$ (1:1) at 110°C for 1.5 h, affording **9** in 68% yield.

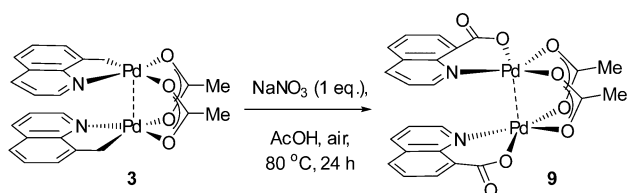


Figure 9. Direct reaction of palladacycle 3 with NaNO_3 .

The minor species present by ^1H NMR (see Figure 6) were of concern to us, particularly as they could not be satisfactorily characterized with the data available. ^{15}N labeling was therefore employed to pursue possible $\text{Pd}-\text{NO}_x$ interactions in these minor species. In an otherwise equivalent reaction, palladacycle 3 was reacted with $\text{Na}^{15}\text{NO}_3$. A $^1\text{H}\{^{15}\text{N}\}$ HMQC experiment allowed two clear nitrogen chemical environments (at δ 269 and 340 ppm) to be proton correlated. The major signal observed at δ 6.08 ppm correlates with the ^{15}N signal at δ 340 ppm (Figure 10). A weaker long-range $^1\text{H}-^{15}\text{N}$ coupling was seen between δ 340 ppm and δ 8.85 ppm (H_{Quin}), overlapping

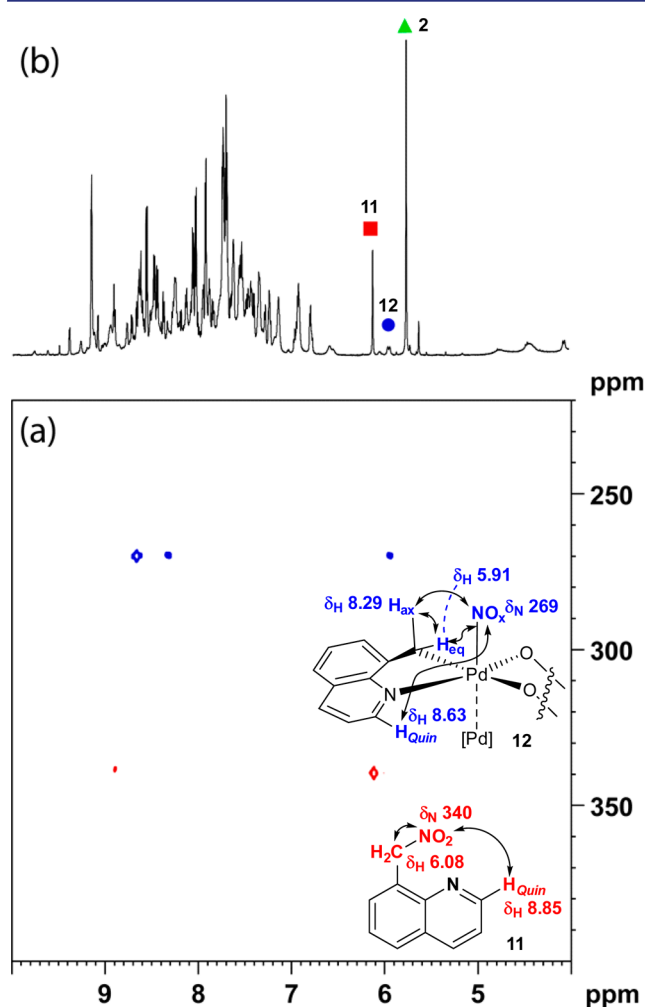


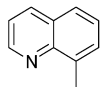
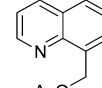
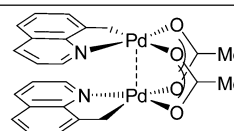
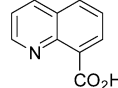
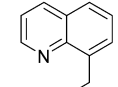
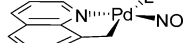
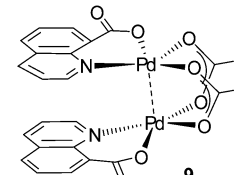
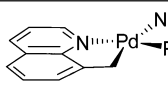
Figure 10. (a) $^1\text{H}\{^{15}\text{N}\}$ HMQC NMR spectrum (700 MHz) from the reaction of 3 with $\text{Na}^{15}\text{NO}_3$ in $\text{AcOH}-d_4$ after 100 min at 80°C . A 1D ^1H spectrum (b) provides a more accurate reflection of the populations of the two $^{15}\text{NO}_x$ species; $\delta(^1\text{H})$ 6.08 ppm (red square, 11); $\delta(^1\text{H})$ 5.91 ppm (blue circle, $\text{Pd}-\text{NO}_x$ complex) and $\delta(^1\text{H})$ 5.72 ppm (green triangle, 2). Note: the signal at 5.72 ppm is shown off scale.

with other species). The ^{15}N signal at δ 269 ppm correlates with δ 5.91 and δ 8.29 from the diastereotopic hydrogens of a CH_2 (vide infra) and 8.63 (H_{Quin}). Both of these nitrogen shifts are within the expected range for $\text{M}-\text{ONO}_2$, $\text{M}-\text{NO}_2$, and $\text{R}-\text{NO}_2$ species,²⁸ and the observed signal-to-noise ratio requires that both species are derived from the $\text{Na}^{15}\text{NO}_3$ and cannot be from the quinoline ligand which is at natural abundance (see the Supporting Information).

A repeat experiment to monitor the reaction using natural abundance NaNO_3 reveals the ^1H signal at 6.08 ppm to be a singlet rather than a doublet (2.1 Hz) and the signal at 5.91 ppm also shows evidence of additional unresolved coupling in the reaction with $\text{Na}^{15}\text{NO}_3$.

To assist with the characterization of this species, $^{14}/^{15}\text{N}$ NMR spectral data (natural abundance) for a series of compounds (in both CDCl_3 and $\text{AcOH}-d_4$) of interest to this study were collected (Table 1).

Table 1. ^{15}N NMR Data for Selected Compounds in This Study (298 K)

Compound	$\delta^{15}\text{N}$ (ppm)	solvent
$\text{Na}^{15}\text{NO}_3$	374	$\text{AcOH}-d_4$
 1	230	$\text{AcOH}-d_4$
	306	CDCl_3
 2	274	$\text{AcOH}-d_4$
 3	- ^a	$\text{AcOH}-d_4$
	233	CDCl_3
 10	231	$\text{AcOH}-d_4$
	275	CDCl_3
 11	284 (N_{quin}), 340 (NO_2)	$\text{AcOH}-d_4$
	296 (N_{quin}), 340 (NO_2)	$\text{AcOH}-d_4$
 7b, L = CH_3CN 7b', L = $\text{AcOH}-d_4$	233 (N_{quin}), 245 (MeCN) 312 (NO_2) ^b	CDCl_3
	- ^c	$\text{AcOH}-d_4$
	180	CDCl_3
 9	-	$\text{AcOH}-d_4$
	255 (N_{quin}), 305 (ONO_2) ^b	CDCl_3
 6a	255 (N_{quin}), 305 (ONO_2) ^b	CDCl_3

^aNo ^{15}N signal observed due to dynamic behavior. ^bNitrogen shift measured from 1D ^{14}N spectrum. ^cInsoluble material.

The ^{15}N chemical shift of NO_3^- is δ 374 ppm in $\text{AcOH-}d_4$. The quinoline nitrogen (N_{quin}) is typically found in the region δ 230–233 ppm (in $\text{AcOH-}d_4$) in compounds **1**, **3**, and **10**, whereas it is δ 274 ppm for compound **2**. The ^{15}N chemical shifts were higher in CDCl_3 than $\text{AcOH-}d_3$ as at the lower pH the quinoline is in equilibrium with the quinolinium ion.²⁹ Therefore, the ^{15}N chemical shift of complex **9** of δ 180 ppm in CDCl_3 is likely lower in $\text{AcOH-}d_4$; the latter solvent could not be used due to the poor solubility of **9**. The ^{15}N NMR chemical shifts are in keeping with those recently described by Stahl and co-workers.³⁰ At natural abundance, no $^1\text{H-}^{15}\text{N}$ correlation could be observed for the NO_2 of **7b**; however, the 1D ^{14}N (see the Supporting Information) in CDCl_3 reveals a chemical shift of 312 ppm for the Pd-NO_2 . In AcOH , **7b** is catalytically active and slowly produces **2** (1–2 days). $^1\text{H}\{^{15}\text{N}\}$ HMQC spectra (under these conditions revealed a signal δ 340 ppm (^{15}N), which correlates with the methylene protons at δ 6.08 ppm. The observation of the same intermediate, as in the reaction of **3** with $\text{Na}^{15}\text{NO}_3$, indicates that this species must be formed via a Pd-NO_2 species.

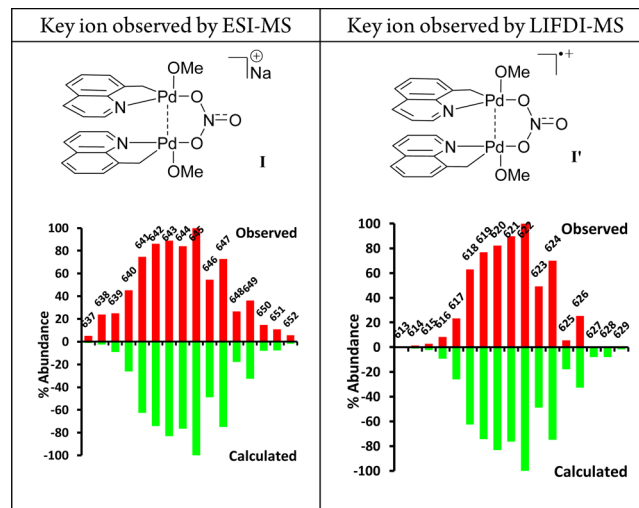
The spectrum of **11** showed $^1\text{H-}^{15}\text{N}$ correlations at δ 6.10, 340 ppm (CH_2 , NO_2) and δ 9.14, 284 ppm ($o\text{-H}_{\text{quin}}$, N_{quin}). Despite the small difference in the ^1H shift (ascribed to pH differences of the solution), we assign the (δ 6.08, 340 ppm) signal to compound **11**.

The signal at δ 5.91 ppm (Figure 10) arises from one of the hydrogens of a diastereotopic CH_2 group. The signal appears as a doublet with a splitting of 15.5 ± 0.2 Hz at 16.4 and 9.4 T (700 and 400 MHz ^1H , respectively). 1D ^1H exchange spectra ($t_{\text{mix}} = 0.3$ s) upon selective irradiation of the signal at 5.91 ppm revealed a signal at δ 8.29 ppm which appears as a doublet with a splitting of 15.5 Hz and is of the same phase as the selectively irradiated signal indicating that it arises due to chemical (EXSY) rather than spin–spin exchange (NOE). A multiplicity-edited $^1\text{H}\{^{13}\text{C}\}$ HSQC (see the Supporting Information), indicated that both of these hydrogens were attached to “ CH_2 -type” carbons and within the resolution of the experiment, both were attached to the same carbon (78.0 ± 0.3 ppm). The very high chemical shift of δ 8.29 ppm could be explained by H-bonding with the NO_x anion. The only other compound where the methylquinoline CH_2 was found to be diastereotopic was the dimeric palladacycle **3** (*anti*-isomer: δ 2.56 and 3.47 ppm, $^2J = 12.9$ Hz, *syn*-isomer: δ 3.41 and 3.77 ppm, $^2J = 8.5$ Hz). In order to gauge the relative size (solvodynamic radius) of the compound giving rise to the signal at 5.91 ppm, a 2D diffusion-ordered (DOSY) spectrum was collected. The known species in the reaction mixture (**2**, **11**, and $\text{AcOD-}d_4$) had diffusion coefficients of $4.21 \times 10^{-10} \text{ m}^2 \text{ s}^{-1}$, $4.92 \times 10^{-10} \text{ m}^2 \text{ s}^{-1}$, and $8.04 \times 10^{-10} \text{ m}^2 \text{ s}^{-1}$, respectively. The signal at 5.91 ppm was found to arise from a complex with a much lower diffusion coefficient, $D = 2.69 \times 10^{-10} \text{ m}^2 \text{ s}^{-1}$, indicating it is of significantly larger size.

ESI-MS and LIFDI-MS analysis. Electrospray ionization mass spectrometry (ESI-MS³¹) is a useful tool for characterizing charged organometallic compounds. Liquid injection field desorption ionization mass spectrometry (LIFDI-MS³²) can also be used to characterize neutral organometallic species. Both ESI-MS and LIFDI-MS are soft ionization methods, making them suitable for detecting Pd species present under working reaction conditions. Xu and co-workers successfully detected Pd intermediates by ESI-MS in their C–H bond fluorination chemistry.⁷ The direct ESI-MS analysis of the reaction of palladacycle **3** with NaNO_3 in AcOH at 50 °C was

conducted. Dissolution of reaction samples in MeOH before electrospray injection facilitated effective ionization. Analysis of a sample after 1 h reaction revealed the presence of a sodiated dinuclear Pd ion **I** that contains the cyclometalated backbone at Pd, suggesting that it possesses $\mu\text{-1,3-NO}_3$ and two terminal OMe ligands (Table 2). The observed and calculated isotope patterns for the proposed structures are gathered in Table 2.

Table 2. ESI-MS and LIFDI-MS Analysis of the Reaction of **3** with NaNO_3 in AcOH at 50 °C at 1 h^a



^aThe structures are suggested for key molecular ion peaks observed by ESI-MS and LIFDI-MS (**I** = $[\text{C}_{22}\text{H}_{22}\text{N}_3\text{O}_5\text{Pd}_2\text{Na}]^+$ and **I'** = $[\text{C}_{22}\text{H}_{22}\text{N}_3\text{O}_5\text{Pd}_2]^+$), and it is feasible that the methoxy/ NO_3 ions could occupy different positions and offer bridging or terminal coordination to Pd.

A radical cation **I'** was observed by LIFDI-MS, which provides support for these higher oxidation state Pd species containing a nitrate ligand. At 1.5 h, other ions were observed, including a partially oxidized dinuclear Pd species by ESI-MS, which supports the formation of complex **9** under working reaction conditions and consistent with the NMR studies (see the Supporting Information). After 2 h, the major ions observed by ESI-MS and LIFDI-MS were derived from **9**. Other ions were detected under the working reaction conditions, for which attempts to fit reasonable structures and chemical formulas were unsuccessful.

Reaction Kinetics and Appearance of Gases under Working Catalyst Conditions. The originally reported reaction of **1** \rightarrow **2**, mediated by $\text{Pd}(\text{OAc})_2$ and 1 equiv of NaNO_3 , in air-saturated AcOH , was conducted for 18 h at 110 °C (Figure 11).³ We learned that this reaction was over within minutes at this temperature. Lowering the reaction temperature to 80 °C allowed the evolution of product **2** to be monitored by GC analysis (temperature at $t = 0$ min was 80 °C). In all cases, classical homogeneous behavior is apparent and there is no evidence to suggest the involvement of Pd nanoparticles (heterogeneous processes) under these oxidizing conditions.³³ The reaction mediated by $\text{Pd}(\text{OAc})_2$ reaches 94% conversion after 10 min. The catalytic competency of the presynthesized complexes **3**, **7a**, **7b**, **8**, and **9** was established under conditions otherwise identical to those of $\text{Pd}(\text{OAc})_2$. It is apparent that the kinetics observed for the reaction mediated by $\text{Pd}(\text{OAc})_2$ are different from that mediated by **9**. The appearance of a defined induction period suggests that **9** is a precatalyst. The initially

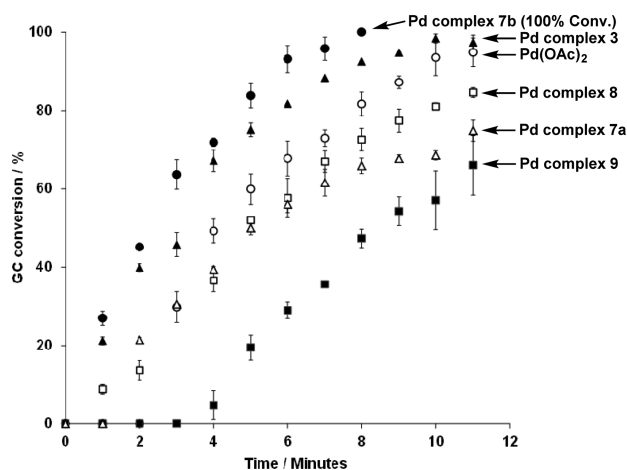


Figure 11. Kinetic plots for the reaction of **1** \rightarrow **2** catalyzed by Pd(OAc)₂ (5 mol % Pd) and complexes **3**, **7a**, **7b**, **8**, and **9** (1 equiv of NaNO₃, 80 °C, air-saturated AcOH). Reactions with dinuclear Pd complexes employed 10 mol % Pd. Each data point is an average of three independent GC injections (error bars for each conversion point are shown against each curve).

formed palladacycle **3** and *trans*-Pd(OAc)₂(**2**)₂ **8** share catalytic activity that is commensurate with Pd(OAc)₂. Within the series, the most active catalyst was **7b**, containing an NO₂ anion, which was found to be more active than the corresponding catalyst **7a** containing an NO₃ anion.

In reactions of **1**, mediated by Pd(OAc)₂ in the presence of 1 equiv of NaNO₃, the evolution of NO is seen on heating between 80 and 110 °C. The appearance of a red/brown gas is visible after \sim 2 min reaction time, which is attributed to NO₂ \uparrow vide infra. Infrared spectroscopic analysis of the catalytic reaction **1** \rightarrow **2** under working conditions at 80 °C (under air) revealed that two new bands at 2213 and 2178 cm⁻¹ grew in after 2 h reaction time (see the [Supporting Information](#)). These bands were attributed to N₂O,³⁴ the formation of which occurs on full consumption of substrate **1**.

Gas headspace analysis, using a customized chemiluminescence NO_x analyzer (see the [Experimental Section](#)), of the reaction of **1** \rightarrow **2** catalyzed by Pd(OAc)₂ in the presence of 1 equiv of NaNO₃, allowed the gases evolved to be characterized. It was necessary to run a reaction using 2.3 mmol of **1** in AcOH/Ac₂O (40 mL, 7/1, v/v), giving a concentration in **1** of 0.0575 M. The gases were analyzed directly from the top of the reaction condenser, equipped with a glass tubing-based piece allowing the entrance of a flux of “zero-air” and the exit of the gases to the detectors. The volume dilution was 15 L min⁻¹. The reaction was started at 25 °C, as the large volume of AcOH/Ac₂O would require ca. 20 min to reach 110 °C. The experiment conducted in this way showed that mixing **1**, Pd(OAc)₂, and NaNO₃ in AcOH/Ac₂O led to the evolution of NO_x gases at 25 °C (depicted as product evolution curves in [Figure 12](#)). The concentrations of NO_x gases reported are given as mixing ratios, in parts per million. The total amount of NO_x formed is ca. 140 ppm (\sim 1.2 mmol), consuming over half of the NaNO₃ (2.3 mmol) initially present. The experiment confirms that NO is formed rapidly under these reactions. NO₂ also forms, which continues to increase at the expense of NO; therefore, as demonstrated by this experiment, air (O₂) is playing the role of reoxidant.

The interaction of nitrate with air in light could also lead to the formation of O₃. However, there was no clear evidence that

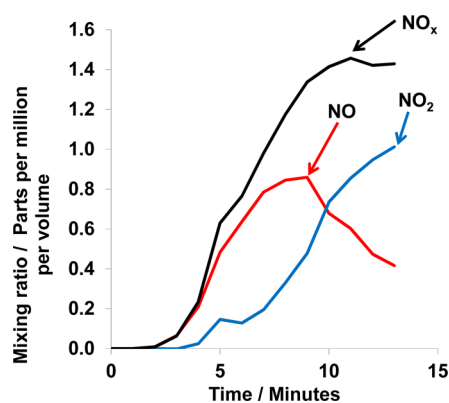


Figure 12. Head-space analysis of the reaction **1** \rightarrow **2**, mediated by Pd(OAc)₂ (5 mol %) and NaNO₃ (1 equiv) in AcOH/Ac₂O ($t_0 = 25$ °C), with heating to 110 °C (over 15 min) (note: NO_x = NO + NO₂).

light affected the catalytic chemistry (cf. only a marginal difference in acetoxylation reaction kinetics was recorded). Moreover, the formation of O₃ was not detected under these reaction conditions.

Following on from the results gained by the headspace analysis, we tested the reaction **1** \rightarrow **2**, mediated by Pd(OAc)₂ (5 mol %) and NaNO₃ (1 equiv) in AcOH at room temperature, which gave **2** in 90% conversion after 3 days.

A preparative-scale reaction of **2**, catalyzed by 5 mol % Pd(OAc)₂, 1 equiv of NaNO₃ in AcOH/Ac₂O at 110 °C, gave liberated acid **10** in 23% yield ([Figure 13](#)). Future studies will



Figure 13. Example demonstrating the feasibility of a catalytic reaction **2** \rightarrow **10**.

address the feasibility of this catalytic transformation in more general terms, e.g., in terms of substrate scope, as it has the potential to be synthetically useful.

Lastly, reaction of **7b** with NO₂ gas was conducted as, based on literature precedent,³⁵ we envisaged that the NO₂ ligand at Pd^{II} could be oxidized to NO₃ ([Figure 14](#)).

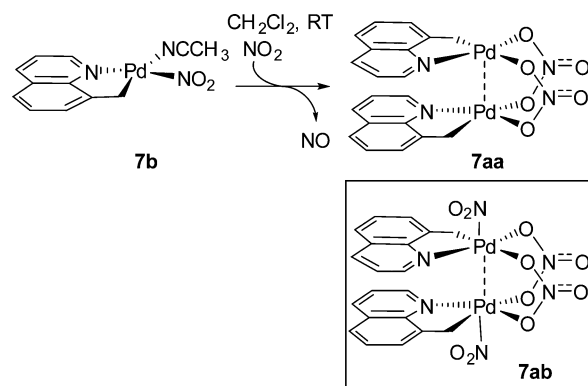


Figure 14. Reaction of **7b** with NO₂ (gas) monitored by in situ infrared spectroscopic analysis (ReactIR): tentatively suggested oxidized Pd complexes.

Bubbling a CH_2Cl_2 solution of **7b** with NO_2 led to loss of CH_3CN from **7b**. Reaction monitoring by in situ spectroscopic analysis allowed us to visualize solubilization of NO_2 (g) (saturated at ca. $t = 5$ min), loss of **7b**, and formation of a new compound (Figure 15). On the basis of the IR data, a

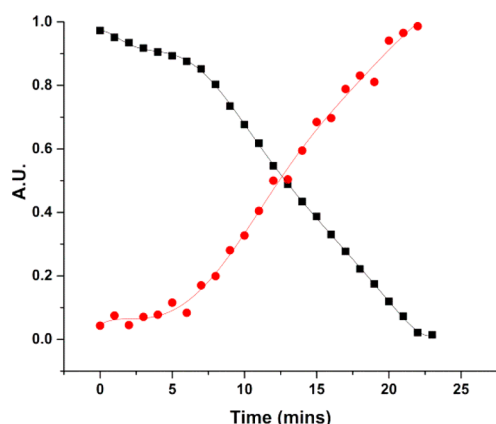


Figure 15. In situ IR reaction monitoring of **7b** \rightarrow **7aa** in the presence of NO_2 (g) (1251 cm^{-1}) at $20\text{ }^\circ\text{C}$. The black dots show depletion of **7b** at 1223 cm^{-1} , and red dots show appearance of **7aa** at 717 cm^{-1} .

dinuclear Pd complex possessing two μ -1,3- NO_3 ligands (**7aa**) is tentatively proposed, based on a characteristic deformation mode at 717 cm^{-1} , assigned to μ -1,3- NO_3 , similar to a related complex reported by Yu et al. (766 cm^{-1}).²¹ Extensive analysis by LIFDI was unable to reveal the molecular ion of **7aa**, although a very weak molecular ion for **7ab** was found (see the Supporting Information). The ^1H NMR spectra of this complex suggest that the quinoline protons have become highly deshielded (distinct from nitrated organic product **11**), in keeping with the structure proposed containing NO_3 anions.

DISCUSSION AND CONCLUSION

From this study, evidence supporting the role of nitrate and nitrite anions at Pd in the aerobic Pd-catalyzed oxidation of nonactivated $\text{sp}^3\text{-C-H}$ bonds has been gathered. 8-Methylquinoline **1** was identified as a model substrate to conduct this study, which affords acetoxylation product **2**, and was originally reported in Sanford's work³ as part of an expanded substrate scoping study.

The findings include (all catalytic processes refer to the reaction of **1** \rightarrow **2** conducted at $110\text{ }^\circ\text{C}$ in $\text{AcOH}/\text{Ac}_2\text{O}$, unless specified) the following:

- Cyclopalladation of **1** with $\text{Pd}(\text{OAc})_2$ affords a dinuclear Pd complex **3** (in AcOH), which is catalytically competent.
- Palladacycles containing NO_3 and NO_2 ligands (**7a** and **7b**, respectively) are both viable (pre)catalysts.
- Palladacycle **7a** functions as an active catalyst in the absence of additional NaNO_3 co-catalyst.
- Under either N_2 or air, a catalytic reaction mediated by **1** equiv of $\text{NaN}^{18}\text{O}_3$ showed incorporation of the ^{18}O label into acetoxylation product **2** (in AcOH). Negligible ^{18}O incorporation was recorded under O_2 .
- Stoichiometric reactions of **3** with NaNO_3 at either 50 or $80\text{ }^\circ\text{C}$ revealed the intermediacy of several species – *trans*- $\text{Pd}(\text{OAc})_2(\text{2})_2$ (**8**) and the oxidized Pd complex **9** could be characterized (in $\text{AcOH-}d_4$). The latter complex formed quantitatively, after overnight heating at $80\text{ }^\circ\text{C}$.

- Another intermediate from (e) was revealed by stoichiometric reaction of **3** with $\text{Na}^{15}\text{NO}_3$, proposed as being a Pd-containing species possessing a NO_x ligand.
- The formation of nitrated product **11** has been observed in stoichiometric reactions of **3** and NaNO_3 in acetic acid, which is converted to acetoxylation product **2**, in the presence of Pd at $50\text{ }^\circ\text{C}$, and in the absence of Pd at $110\text{ }^\circ\text{C}$.
- ESI-MS and LIFDI-MS provided indirect evidence for the formation of dinuclear palladacycles containing NO_3 anion (with AcOH/MeOH), which also confirmed the evolution of an oxidized ligand backbone (leading to the isolation of **9**).
- Complex **9** is catalytically competent and exhibits an induction period, contrasting with the catalytic behavior of the other Pd complexes (**3**, **7a**, **7b**, and **8**).
- The in situ infrared spectroscopic analysis of a catalytic reaction catalyzed by $\text{Pd}(\text{OAc})_2$ at $80\text{ }^\circ\text{C}$ showed the evolution of N_2O , after prolonged heating (up to 12 h).
- Head-space analysis of a catalytic reaction, started at $25\text{ }^\circ\text{C}$ and heated to $110\text{ }^\circ\text{C}$, revealed the rapid formation of NO and NO_2 gases within 2 min. The formation of NO and subsequent oxidation to NO_2 , confirms that NO is being oxidized under the aerobic reaction conditions.
- The mechanistic observations made above allowed identification of a room temperature catalytic reaction (90% conversion to **2**, over 3 days, was recorded).

Based on the above evidence, a catalytic cycle involving dinuclear palladacycle **3** as an entry point is plausible. The precise redox chemistry involving NO_3 and NO_2 anions at Pd is undoubtedly complicated. Direct evidence for NO_3 and NO_2 anions acting as ligands at Pd^{II} has been obtained (by X-ray diffraction, NMR spectroscopy, and MS analysis). Transfer (exchange) of ^{18}O from $\text{NaN}^{18}\text{O}_3$ into the acetoxylation product **2** confirms that ^{18}O exchange between NO_3 and OAc anions occurs at Pd, which is in keeping with the observations made by Bäckvall and co-workers in the acetoxylation/hydration reactions of olefins.¹⁵

The presence of nitrated product **11** indicates that NO_2 is acting as a ligand at Pd and that reductive elimination is feasible. Moreover, such products are intermediates to acetoxylation product **2**.

The formation of complex **9** indicates that the reaction of **1** \rightarrow **2** is running under strongly oxidizing conditions. Prolonged heating will therefore lead to loss of product **2**, impacting on overall yield. The primary reason for this is that *trans*- $\text{Pd}(\text{OAc})_2(\text{2})_2$ (**8**) goes on to form complex **9** under the reaction conditions.

NO_x gases readily evolve in the aerobic Pd-catalyzed oxidation of nonactivated $\text{sp}^3\text{-C-H}$ bonds.³ Our headspace measurements indicate that NO is rapidly formed under working reaction conditions, with measurements starting at room temperature. We believe that the solubility of NaNO_3 is critical here, where higher temperatures favor dissolution.

Oxidation of Pd- NO species to Pd- NO_2 and Pd- NO_3 species is reported,³⁶ and there is an interesting complementarity here with iron-nitrato/iron-nitrosyl chemistry.^{37,16b}

The formation of N_2O is noted on prolonged heating and reaction times (by in situ IR measurements). We cannot identify a clear role for N_2O , other than it is a dead-end for catalysis, which is in keeping with the timing of its appearance, long after substrate turnover has completed. N_2O formation

can be explained by dimerization of HNO as a termination reaction.³⁸

We propose a mechanism involving higher oxidation state Pd species (Figure 16). It is unclear whether Pd^{IV} species are

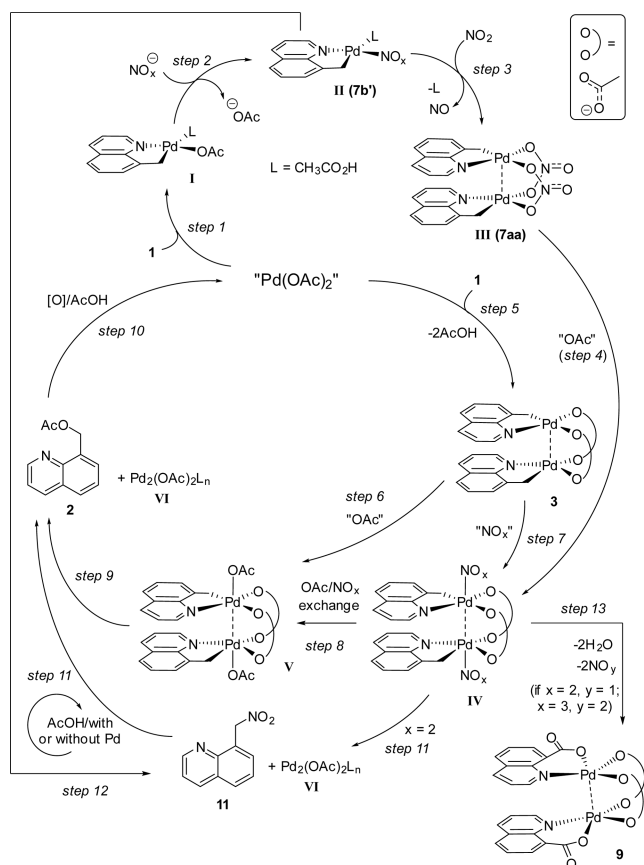


Figure 16. Postulated mechanism based on the experimental evidence gathered in this study (where OAO is shown as acetate, the bridging ligand could also be nitrate).

involved in these transformations—with the experimental evidence available, we propose that dinuclear Pd^{III} species play an important role in catalysis, which is based on the combined NMR, MS, and IR data that we have available from this study. The mechanism makes the reasonable assumption that Pd₃(OAc)₆ breaks down to form Pd(OAc)₂ under the reaction conditions. The caveat to our hypothesis is that structurally characterized Pd^{IV} species containing NO, NO₂, and NO₃ and tris(pyrazolyl)borate ligands have been reported by Cámpora and co-workers.³⁹ These model systems are of potential relevance to the catalytic C–H acetoxylation reaction mechanism, particularly as oxygen was shown to oxidize a Pd^{IV}–NO complex to Pd^{IV}–NO₃.

Cyclopalladation can occur through either monomer or dimer complexes (Figure 16, steps 1 and 5), a proposal supported by Musaev's recent study.⁴⁰ NO₂[−]/NO₃[−] metathesis is facile at Pd, as demonstrated by experiment (step 2). Species II can either react with liberated NO₂ to give III or directly form 11 by reductive elimination (indicated as step 12). Species III can then be directly oxidized under the reaction conditions to give IV (step 7), a species speculated by Liu and co-workers as being formed in reactions employing *tert*-butyl nitrite.⁴¹ The experimental evidence, particularly the ¹⁵N NMR evidence, tentatively supports such type of an intermediate being formed

under the reaction conditions. Intermediate IV can also derive from NO₂ oxidation of validated dimer intermediate 3 (step 7). It is further recognized that NO_x-free intermediates could form under the conditions, either by oxidation of 3 (step 6) or anion metathesis with IV (step 8), giving V. Against this latter proposal are the ¹⁸O-labeling studies indicating that NO_x is at Pd for oxygen exchange to occur intramolecularly with acetate (¹⁸O appearing in product 2). Reductive elimination from V gives acetoxyated product 2 (step 9) and a Pd species that requires reoxidation to Pd(OAc)₂ (step 10), which is feasible under the oxidizing conditions of the reaction. The nitrated organic product 11 can form directly from IV, in keeping with that proposed.³⁸ Here, a Pd reoxidation step is again necessary, akin to step 10 (not shown). Step 11 shows how nitrated organic product 11 can be converted into 2, confirmed by experiment as being more rapid in the presence of Pd, although it occurs without.

We regularly encountered formation of complex 9 in our studies, which can derive from IV by oxidation of the methylene group to a carbonyl (step 13). The characterization of the potential intermediate 12, from the ¹⁵N NMR labeling studies, provides support for this hypothesis—the very high chemical shift for a methylene proton (δ 8.29 ppm) indicates an interaction of an NO_x anion (at Pd), which can ultimately assist this oxidation step.

To conclude, the principal aim of this investigation was to delineate the role played by nitrate and nitrite anions in the aerobic Pd-catalyzed oxidation of nonactivated sp³-C–H bonds. Here, we were able to draw on the promising methodology described by Sanford³ and other Pd-catalyzed processes taking advantage of such redox anions.^{8,9} Recent synthetic developments,^{5,7} when taken together with the mechanistic work described herein, serve to highlight the potential of redox active anions such as nitrate and nitrite in oxidative Pd-catalyzed processes. The approach taken to testing the catalytic viability of suitable Pd–NO_x complexes will, we hope, be more widely adopted by others in studying Pd/NO_x-mediated organic transformations, which may also prove useful in understanding regiochemical consequences in appropriate transformations. The intimate role of NO_x at Pd is undoubtedly complicated, but through appropriate isotopic labeling and complementary mechanistic studies, useful experimental evidence can be gathered.

EXPERIMENTAL SECTION

General Experimental and Instrumental Details. Reagents were purchased from Sigma-Aldrich, Alfa Aesar, Acros Organics, or Fluorochem and used as received unless otherwise stated. Isotopically labeled chemicals were purchased from Icon Isotopes, Ltd. and used as received. Pd(OAc)₂ was obtained from Precious Metals Online. Dry THF, CH₂Cl₂, and CH₃CN were obtained from a Pure Solv MD-7 solvent system and stored under nitrogen. THF was also degassed by bubbling nitrogen through the solvent with sonication. Dry methanol was obtained by drying over 3 Å molecular sieves. Petroleum ether refers to the fraction of petroleum that is collected at 40–60 °C. Reactions requiring anhydrous conditions were carried out using Schlenk techniques (high vacuum, liquid nitrogen trap on a standard in-house built dual line). Room temperature upper and lower limits are stated as 13–25 °C, but typically 21 °C was recorded. Brine refers to a saturated aqueous solution of NaCl.

Thin-layer chromatography (TLC) was carried out using Merck 5554 aluminum-backed silica plates (silica gel 60 F254), and spots were visualized using UV light (at 254 nm). Where necessary, plates were stained and heated with one of potassium permanganate, anisaldehyde or vanillin as appropriate. Retention factors (Rf) are

reported in parentheses along with the solvent system used. Flash column chromatography was performed according to the method reported by Still et al.⁴² using Merck 60 silica gel (particle size 40–63 μm) and a solvent system as reported in the text.

NMR spectra were obtained in the solvent indicated using a JEOL ECX400 or JEOL ECS400 spectrometer (400, 101, and 162 MHz for ^1H , ^{13}C , and ^{31}P , respectively) or a Bruker 500 (500, 126, and 202 MHz for ^1H , ^{13}C , and ^{31}P , respectively). Chemical shifts are reported in parts per million and were referenced to the residual nondeuterated solvent of the deuterated solvent used (CHCl_3 TMH = 7.26 and TMC = 77.16 (CDCl_3), CDHCl_2 TMH = 5.31 and TMC = 54.0 (CD_2Cl_2), $(\text{CHD}_2)\text{SO}(\text{CD}_3)$ TMH = 2.50 and TMC = 39.52 $\{\text{SO}(\text{CD}_3)_2\}$, ^1H and ^{13}C respectively). $\text{AcOD}-d_4$ was referenced to 2.04 ppm (^1H only). Spectra were typically run at a temperature of 298 K. All ^{13}C NMR spectra were obtained with ^1H decoupling. ^{31}P NMR were referenced internally and recorded with ^1H decoupling. NMR spectra were processed using MestrelNova software (versions 5.3, 7.03 and 8.1). The spectra given below were typically saved as .emf files in MestrelNova and inserted into a Microsoft Word document. For the ^1H NMR spectra, the resolution varies from 0.15 to 0.5 Hz; the coupling constants have been quoted to ± 0.5 Hz in all cases for consistency. ^1H NMR chemical shifts are reported to two decimal places; ^{13}C and ^{31}P NMR chemical shifts are reported to one decimal place (note: for some ^{13}C signals it was necessary to report to two decimal places).

High-field NMR spectra were acquired at 16.4 T on a Bruker Avance II spectrometer equipped with 5 mm TXI or BBO probes. Spectra of natural abundance samples (**1**, **2**, **3**, **7b**, **10**, and **9**) and the monitoring of the reaction of **3** to **2** were acquired using the TXI probe. The monitoring of the reaction of **1** to **2** in the presence of $\text{Na}^{15}\text{NO}_3$ was performed with the BBO probe to facilitate direct observation of ^{15}N species. ^1H NMR spectra (700.13 MHz) were acquired using a Bloch-decay (single-pulse) sequence with a 5 s recycle delay, 15 ppm spectral widths, and 3 s acquisition times that are the sum of 32 coadded transients. $^1\text{H}\{^{15}\text{N}\}$ correlation spectra (700.13 and 70.96 MHz, respectively) were acquired using an HMQC pulse sequence with pulsed field-gradient based coherence selection. Spectra were acquired with different spectral widths and/or transmitter offsets in the ^{15}N dimension in order to ensure detect for possible leasing of signals in the indirect dimension. ^1H chemical shifts are reported relative to TMS, and ^{15}N chemical shifts are reported relative to liquid ammonia.

Infrared spectra were obtained using either a Unicam Research Series FTIR (KBr IR) or a Bruker ALPHA-Platinum FTIR Spectrometer with a platinum–diamond ATR sampling module. Where indicated, reactions were monitored in situ using a Mettler Toledo ReactIR ic₁₀ with a K6 conduit SiComp (silicon) probe and MCT detector.

MS spectra were measured using a Bruker Daltonics micrOTOF MS, Agilent series 1200LC with electrospray ionization (ESI and APCI) or on a Thermo LCQ using electrospray ionization, with <5 ppm error recorded for all HRMS samples. LIFDI mass spectrometry was carried out using a Waters GCT Premier MS Agilent 7890A GC (usually for analysis of organometallic compounds when ESI or APCI are not satisfactory ionization methods). Mass spectral data are quoted as the m/z ratio along with the relative peak height in brackets (base peak = 100). Mass to charge ratios (m/z) are reported in daltons. High-resolution mass spectra are reported with <5 ppm error (ESI) or <20 ppm error (LIFDI). For clarity, LIFDI data are reported for ^{106}Pd , the most abundant natural isotope of Pd.

Melting points were recorded using a Stuart digital SMP3 machine.

Gas chromatographic analysis was carried out using a Varian CP-3800 GC equipped with a CP-8400 autosampler. Separation was achieved using a DB-1 column (30 m \times 0.32 mm, 0.25 μm film thickness) with carrier gas flow rate of 2 mL min^{-1} and a temperature ramp from 50 to 250 $^\circ\text{C}$ at 20 $^\circ\text{C}$ min^{-1} . The injection volume was 1 μL with a split ratio of 10 (details of the kinetics measurements are given below).

The chemiluminescence NO_x analyzer is a custom dual channel instrument from Air Quality Design (AQD, Inc., Golden, CO)

measuring at 1 Hz on both channels simultaneously. Channel 1 (ch1) measures NO and has a nominal sensitivity of 3.5 counts per second/parts per trillion (cps/ppt). Channel 2 (ch2) measures NO_x ($\text{NO} + \text{NO}_2$) by dissociating NO_2 to NO with a photolytic converter (blue light converter) that irradiates the sample gas at 390 nm. The nominal sensitivity on channel 2 is 4 cps/ppt. NO_2 is obtained by subtracting ch1 from ch2. The effective limit of detection is ~ 2.5 ppt/min NO and ~ 6.5 ppt/min NO_2 . Note: ppm values are given in Figure 12. Prechamber zero measurements are taken every 5 min for 30 s. The whole system is kept at 4 Torr vacuum pressure. The sample flow rate is 1 sLpm per channel, MFC controlled. Calibration for sensitivity is done by standard addition of NO; converter efficiency is determined by gas-phase titration (GPT) of NO to NO_2 with O_3 . Artifact is determined in zero air, which is made by taking dried (-40 $^\circ\text{C}$ dew point) compressed air, passing it through 13x molecular sieves, then sofonofil to remove NO_x and through activated carbon to remove ozone and VOCs. The 2B Technologies Model 202 Ozone Monitor is designed to enable accurate and precise measurements of O_3 ranging from low ppb (precision of ~ 1 ppb) up to 100000 ppb (0–100 ppm) based on the absorption of UV light at 254 nm.

All DFT calculations were performed using the TURBOMOLE V5 package using the resolution of identity (RI) approximation.⁴³ Initial optimizations were performed at the (RI)-BP86/SV(P) level, followed by frequency calculations at the same level. All minima were confirmed as such by the absence of imaginary frequencies; energies, geometries, and vibrational frequencies are presented. Single-point calculations on the (RI)BP86/SV(P)-optimized geometries were performed using the hybrid PBE0 functional and the flexible def2-TZVPP basis set. The (RI)PBE0/def2-TZVPP SCF energies were corrected for their zero-point energies, thermal energies (ΔE), and entropies (obtained from the (RI)-BP86/SV(P)-level frequency calculations at 298.15 K, ΔG 298.15). In all calculations, a 28 electron quasi-relativistic ECP replaced the core electrons of Pd. No symmetry constraints were applied during optimizations. Calculated XYZ coordinates, single-point energies, and vibrational spectra are reported in the Supporting Information.

Characterization of Pd Complexes. Dinuclear $\text{Pd}^{\text{II}}-\text{Pd}^{\text{II}}$ Complex **3 [Pd(8-MQ) (OAc) Dimer].** 8-Methylquinoline (186 mg, 1.3 mmol) and $\text{Pd}(\text{OAc})_2$ (291 mg, 1.3 mmol) were suspended in glacial acetic acid (20 mL), refluxed for 1.5 h, and then filtered. Water (150 mL) was added to the filtrate, and the mixture was allowed to sit overnight. The precipitated product was collected by filtration and recrystallized from CH_2Cl_2 /hexane to yield **3** as a bright orange solid as a 2:1 mixture of isomers (342 mg, 85% yield). Crystals suitable for X-ray diffraction were grown by layering of a CH_2Cl_2 solution with pentane: mp 193–195 $^\circ\text{C}$; ^1H NMR (major isomer) (400 MHz, CDCl_3) δ 8.51 (dd, $J = 5.0, 1.5$ Hz, 2H, H2), 7.87 (dd, $J = 8.4, 1.5$ Hz, 2H, H4), 7.22 (dd, $J = 8.3, 5.0$ Hz, 2H, H3), 7.11–6.99 (m, 2H, H5), 6.89 (dd, $J = 8.1, 7.1$ Hz, 2H, H6), 6.70 (dd, $J = 7.1, 1.1$ Hz, 2H, H7), 3.45 (d, $J = 13.8$ Hz, 2H, CH_2), 2.55 (d, $J = 13.8$ Hz, 2H, CH_2), 2.14 (s, 6H, CH_3); ^{13}C NMR (101 MHz, CDCl_3) δ 181.5 (CO), 152.7 (C9), 148.9 (C2), 148.2 (C10), 136.5 (C4), 127.3 (C6), 126.8 (C7), 122.9 (C5), 121.1 (C3), 120.5 (C8), 41.4 (CH_2), 24.5 (CH_3); LIFDI-MS m/z 615.94 (calcd for $\text{C}_{24}\text{H}_{22}\text{N}_2\text{O}_4\text{Pd}_2$, 615.97); ESI-MS m/z 614.9621 (calcd for $\text{C}_{24}\text{H}_{21}\text{N}_2\text{O}_4\text{Pd}_2$ ($[\text{M} - \text{H}]^+$) 614.9620; IR (KBr, cm^{-1}) 3390, 1566, 1504, 1408, 1050, 817, 776, 671. Anal. Calcd for $\text{C}_{24}\text{H}_{22}\text{N}_2\text{O}_4\text{Pd}_2$: C, 46.85; H, 3.60; N, 4.55. Found: low C (46.17); H, 3.59; N, 4.48.

Dinuclear $\text{Pd}^{\text{II}}-\text{Pd}^{\text{II}}$ Complex **4 [Pd(8-MQ) (Cl) Dimer].** To a solution of **3** (265 mg, 0.43 mmol) in acetone (15 mL) was added lithium chloride (73 mg, 1.72 mmol) in distilled water (10 mL), resulting in immediate precipitation of the product. The precipitate was collected by filtration, and washed with methanol/water (1:1 v/v) to yield **4** as a pale yellow powder (195 mg, 80% yield). Pyridine- d_5 was added to an NMR tube containing a sample of complex **4** in CDCl_3 in order to increase its solubility in common NMR solvents. Upon addition of pyridine- d_5 , a yellow solution was formed, presumably due to the formation of the monomeric complex [PdCl(8-MQ) (pyr- d_5)]. Residual pyridine signals have been omitted from the reported NMR data for clarity: mp 249–251 $^\circ\text{C}$; ^1H NMR

(400 MHz, CDCl₃) δ 9.57 (dd, $J = 5.1, 1.5$ Hz, 2H, H₂), 8.10 (dd, $J = 8.3, 1.5$ Hz, 2H, H₄), 7.54–7.50 (m, 2H, H₅) 7.47–7.42 (m, 2H, H₇), 7.38 (dd, $J = 7.3, 7.0$ Hz, 2H, H₆), 7.31 (dd, $J = 5.1, 8.3$ Hz, 2H, H₃) 3.54 (s, 4H, CH₂); ¹³C NMR (101 MHz, CDCl₃) δ 153.1 (C₉), 151.8 (C₁₀), 147.3 (C₈), 137.2 (C₄), 128.7 (C₅), 127.8 (C₆), 127.6 (C₇), 123.5 (C₂), 121.2 (C₃), 30.1 (CH₂); LIFDI-MS m/z 567.90 (calcd for C₂₀H₁₆Cl₂N₂Pd₂ 567.88); IR (KBr, cm⁻¹) 3059, 2919, 2283, 1563, 1505, 1385, 1375, 1316, 1056, 825, 787, 762, 676. Anal. Calcd for C₂₀H₁₆Cl₂N₂Pd₂: C, 42.28; H, 2.84; N, 4.93. Found: C, 41.92; H, 2.65; N, 4.71.

Mononuclear Pd^{II} Complex 5 [Pd(8-MQ)(PPh₃)Cl]. A solution of Pd(8-MQ) (Cl) dimer 4 (290 mg, 0.5 mmol) and PPh₃ (288 mg, 1.1 mmol) in CH₂Cl₂ (20 mL) was stirred at room temperature for 15 min under nitrogen. The reaction mixture was filtered through Celite, and hexane was added to induce precipitation. The product was collected by filtration and recrystallized from CH₂Cl₂/hexane to yield 5 as fine yellow crystals in quantitative yield (579 mg): mp 205–209 °C; ¹H NMR (400 MHz, CDCl₃) δ 9.79 (m, 1H, H₂), 8.27 (dd, $J = 8.3, 1.6$ Hz, 1H, H₄), 7.86–7.77 (m, 6H, Ar–H), 7.58 (d, $J = 7.9$ Hz, 1H, H₅ or H₇), 7.52 (ddd, $J = 8.3, 5.0, 1.2$ Hz, 1H, H₃), 7.46–7.39 (m, 9H, Ar–H), 7.39–7.36 (m, 1H, H₆), 7.29 (dq, $J = 7.2, 1.3$ Hz, 1H, H₅ or H₇), 2.85 (d, $J = 3.8, 2$ Hz); ¹³C NMR (101 MHz, CDCl₃) δ 152.2, 150.4, 148.2, 137.9, 135.0 (d, $J = 11.9$ Hz), 131.6, 131.1, 130.5 (d, $J = 2.6$ Hz), 129.1, 128.4 (d, $J = 10.8$ Hz), 127.7, 123.8, 121.6, 33.4; ³¹P NMR (162 MHz, CDCl₃) δ 35.2; LIFDI-MS m/z 545.05 (calcd for C₂₈H₂₃ClNPPd 545.03). Anal. Calcd for C₂₈H₂₃ClNPPd: C, 61.56; H, 4.24; N, 2.56. Found: C, 61.70; H, 4.12; N, 2.21.

Mononuclear Pd^{II} Complex 6a [Pd(8-MQ)(NO₂)(PPh₃)]. A solution of 5 (250 mg, 0.46 mmol) and silver nitrate (389 mg, 2.29 mmol) in CH₂Cl₂ (20 mL) was stirred at room temperature for 24 h. The reaction mixture was filtered and the filtrate concentrated in vacuo to yield 6a as a pale yellow solid in quantitative yield (280 mg). Crystals suitable for X-ray diffraction were grown by layering of a CH₂Cl₂ solution with cyclohexane: mp 180–183 °C; ¹H NMR (400 MHz, CD₂Cl₂) δ 8.75–8.71 (m, 1H, H₂), 8.39 (dd, $J = 8.3, 1.2$ Hz, 1H), 7.77–7.64 (m, 3H), 7.55–7.36 (m, 16H), 3.04 (d, $J = 4.2$ Hz, 2H); ¹³C NMR (101 MHz, CD₂Cl₂) δ 151.1, 148.8, 147.7, 138.4, 134.2 (d, $J = 11.9$), 133.9 (d, $J = 16.0$ Hz), 130.9 (d, $J = 2.5$ Hz), 129.2, 128.8, 128.7 (d, $J = 11.0$ Hz), 128.0, 124.1, 121.8, 26.8; ³¹P NMR (162 MHz, CD₂Cl₂) δ 33.0; LIFDI-MS m/z 510.04 [M – NO₂] (calcd for C₂₈H₂₃NPPd 510.06); IR (KBr, cm⁻¹) 3054, 1505, 1447, 1384, 1286, 1096, 1021, 825, 786, 751, 696.

Mononuclear Pd^{II} Complex 6b [Pd(8-MQ)(NO₂)(PPh₃)]. A solution of 5 (250 mg, 0.46 mmol) and silver nitrite (352 mg, 2.29 mmol) in CH₂Cl₂ (20 mL) was stirred at room temperature for 24 h. The reaction mixture was filtered and the filtrate concentrated in vacuo to yield 6b as a light brown solid in quantitative yield (315 mg). We noted that complex 6b is sensitive to air and moisture (OPPh₃ formed over time in CDCl₃ solutions of 6b): mp 178–180 °C; ¹H NMR (400 MHz, CD₂Cl₂) δ 8.68 (s, 1H), 8.35 (d, $J = 8.2$ Hz, 1H), 7.77–7.68 (m, 5H), 7.51–7.37 (m, 12H), 7.36–7.30 (m, 1H), 2.72 (s, 2H); ³¹P NMR (162 MHz, dry CD₂Cl₂) δ 32.4; LIFDI-MS m/z 510.03 [M – NO₂] (calcd for C₂₈H₂₃NPPd 510.06); IR (KBr, cm⁻¹) 3055, 2870, 1684, 1569, 1503, 1481, 1431, 1340, 1095, 825, 752, 696. Complex 6b retained 0.25 equiv of AgCl. Further purification led to its decomposition (we were unable to obtain a satisfactory ¹³C NMR data for 6b). Anal. Calcd for C₂₈H₂₃N₂O₂PPd·Ag_{0.25}Cl_{0.25}: C, 56.74; H, 3.91; N, 4.73. Found: C, 56.77; H, 3.95; N, 4.68 (average of two runs).

Mononuclear Pd(II) Complex 7a [Pd(8-MQ)(NO₂)(NCCH₃)]. Complex 4 (140 mg, 0.25 mmol) and silver nitrate (100 mg, 0.6 mmol) were suspended in a mixture of CH₂Cl₂ and CH₃CN (8 mL, 3:1 v/v) and stirred at room temperature for 24 h. The reaction mixture was filtered and the filtrate concentrated in vacuo to yield 7a as a brown solid in quantitative yield (228 mg): mp 139–143 °C; ¹H NMR (400 MHz, CDCl₃) δ 8.64 (dd, $J = 5.2, 1.5$ Hz, 1H, H₂), 8.26 (dd, $J = 8.4, 1.5$ Hz, 1H, H₄), 7.59 (dd, $J = 7.8, 1.3$ Hz, 1H, H₅), 7.53 (dq, $J = 7.1, 1.3$ Hz, 1H, H₇), 7.46 (dd, $J = 7.1, 7.8$ Hz, 1H, H₆), 7.40 (dd, $J = 5.2, 8.4$ Hz, 1H, H₃) 3.69 (s, 2H, CH₂), 2.34 (s, 3H, CH₃); ¹³C NMR (101 MHz, CDCl₃) δ 152.5 (C₂), 149.7 (C₉), 146.5 (C₈), 138.4 (C₄), 129.0 (C₆), 128.5 (C₇), 128.3 (C₅), 124.2 (C₃), 121.7

(CN), 23.0 (CH₂), 3.6 (CH₃); LIFDI-MS m/z 309.98 [M – NCCH₃] (calcd for C₁₀H₈N₂O₃Pd 309.96); IR (KBr, cm⁻¹) 2924, 2853, 2253, 1732, 1508, 1438, 1384, 1290, 1027, 824, 783, 327.

Mononuclear Pd^{II} Complex 7b [Pd(8-MQ)(NO₂)(NCCH₃)]. Method A, starting from 4 and AgNO₂: Complex 4 (140 mg, 0.25 mmol) and silver nitrite (91 mg, 0.6 mmol) were suspended in a mixture of CH₂Cl₂ and CH₃CN (8 mL, 3:1 v/v) and stirred at room temperature for 24 h. The reaction mixture was filtered, and the filtrate concentrated in vacuo to afford 7b as a yellow solid in quantitative yield (235 mg). Method B, starting from 3 and NaNO₂: Complex 3 (105 mg, 0.171 mmol) and sodium nitrite (118 mg, 1.710 mmol) were suspended under argon in distilled CH₃CN (5 mL) and stirred at reflux for 6 h. The reaction mixture was filtered while hot under argon. Yellow crystals suitable for X-ray diffraction were grown in the filtrate when cooled. The crystals were isolated by filtration and dried to yield 7b in 61% yield (71 mg): mp 239–242 °C; ¹H NMR (400 MHz, CDCl₃) δ 8.53 (dd, $J = 5.0, 1.5$ Hz, 1H, H₂), 8.29 (dd, $J = 8.4, 1.5$ Hz, 1H, H₄), 7.66–7.57 (m, 2H, H₅+H₇), 7.49 (t, $J = 7.6$ Hz, 1H, H₆), 7.43 (dd, $J = 8.4, 5.0$ Hz, 1H, H₃), 3.94 (s, 2H), 2.01 (s, 3H); ¹³C NMR (101 MHz, CDCl₃) δ 152.6 (C₂), 149.6 (C₉), 147.2 (C₈), 138.7 (C₄), 129.4 (C₆), 129.2 (C₇), 128.8 (C₅), 127.9 (C₁₀), 124.4 (C₃), 121.8 (CN), 27.2 (CH₂), 2.1 (CH₃); LIFDI-MS m/z 589.85 [2M – 2CH₃CN] (calcd for C₂₀H₁₆N₄O₄Pd₂ 589.93), 389.06 [M – NO₂ + 8-MQ] (calcd for C₂₀H₁₆N₂Pd 390.03); IR (KBr, cm⁻¹) 2919, 2849, 1505, 1435, 1374, 1216, 1055, 1018, 818, 778.

Mononuclear Pd^{II} Complex 8. Method A, starting from 3 and NaNO₂: Complex 3 (31.7 mg, 0.052 mmol) and NaNO₂ (4.4 mg, 0.052 mmol) were suspended in glacial acetic acid (5 mL) and heated at 50 °C for 1 h. The resulting solution was filtered and concentrated under vacuum. Layering a solution of the previous powder dissolved in CH₂Cl₂ by pentane led to cocrystallization of 8 as orange crystals and 9 as green crystals. Method B, starting from Pd(OAc)₂ complex and 2: Pd(OAc)₂ (53.9 mg, 0.24 mmol) and 2 (91 mg, 0.48 mmol) were suspended in distilled CH₂Cl₂ (5 mL) under argon and mixed at room temperature for 6 h. The resulting solution was layered by distilled pentane (15 mL), and the flask was allowed to sit overnight at 4 °C. The precipitate was filtered and dried under vacuum to afford complex 9 as a green-brown powder. Crystals suitable for X-ray diffraction were directly obtained by layering a solution of 9 in CH₂Cl₂ by pentane. Selected data from a single crystal (from X-ray): ¹H NMR (400 MHz, CDCl₃) δ 8.96 (dd, $J = 4.2, 1.7$ Hz, 2H, H₂), 8.18 (dd, $J = 8.3, 1.7$ Hz, 2H, H₄), 7–85–7.75 (m, 4H, H₅+H₇), 7.55 (dd, $J = 8.2, 7.1$ Hz, 2H, H₆), 7.44 (dd, $J = 8.3, 4.2$ Hz, 2H, H₃), 5.86 (s, 4H), 2.28 (s, 3H), 2.21 (s, 6H), 1.96 (s, 3H).

Dinuclear Pd^{II}–Pd^{II} Complex 9. Method A, starting from 3 and NaNO₂: Complex 3 (115 mg, 0.19 mmol) and NaNO₂ (16 mg, 0.19 mmol) were suspended in glacial acetic acid (10 mL) and heated at 80 °C for 3 h. The resulting solution was filtered and concentrated under vacuum to afford complex 8 as an orange powder in quantitative yield (134 mg). Method B, starting from Pd(OAc)₂ complex and 8-quinolinecarboxylic acid 10: Pd(OAc)₂ (104 mg, 0.46 mmol) and 8-quinolinecarboxylic acid 10 (80 mg, 0.46 mmol) were suspended in glacial acetic acid (10 mL) and heated at 110 °C for 1.5 h. The resulting solution was filtered and poured into cold distilled water (200 mL). The flask was left overnight at 4 °C. The mixture was concentrated under vacuum to induce precipitation of the product. The precipitate was filtered and dried under vacuum to afford complex 8 as an orange powder with 68% yield (106 mg). Crystals suitable for X-ray diffraction were directly obtained from the concentrated solution of 8 in AcOD (NMR tube): ¹H NMR (400 MHz, CDCl₃) δ 8.76 (dd, $J = 5.5, 1.6$ Hz, 2H, H₂), 8.46 (dd, $J = 8.2, 1.6$ Hz, 2H, H₄), 8.01 (dd, $J = 7.4, 1.6$ Hz, 2H, H₅), 7.86 (dd, $J = 8.1, 1.7$ Hz, 2H, H₇), 7.58 (dd, $J = 8.2, 5.5$ Hz, 2H, H₃), 7.31 (t, $J = 7.7$ Hz, 2H, H₆), 2.12 (s, 6H, CH₃); ¹³C NMR (101 MHz, CDCl₃) δ 186.2 (CO, Bn), 172.3 (CO, AcO), 166.8 (C₁₀), 154.6 (C₂), 141.8 (C₄), 138.1 (C₅), 132.8 (C₇), 129.6 (C₆), 127.4 (C₃), 123.8 (C₈), 122.0 (C₉), 24.0 (CH₃); LIFDI-MS m/z 450.93 (calcd for C₂₀H₁₂N₂O₄Pd₁ ([M–Pd–2OAc]) 450.99); ESI-MS m/z 698.9075 (calcd for C₂₄H₁₈N₂O₈Pd₂ ([M + Na]⁺) 698.9079); IR (ATR, cm⁻¹) 3399, 3064, 1722, 1563, 1416, 1333, 1304, 769, 697.

Catalytic Evaluation of the Complexes in the Acetoxylation

Reaction of 1. General procedure A, acetoxylation of 8-methylquinoline **1** under air: To a microwave flask containing Pd precatalyst (0.0125 mmol, 5 mol % with respect to substrate) and NaNO₃ (0–1 equiv relative to substrate) was added 2 mL of AcOH/Ac₂O (7:1). 8-Methylquinoline **1** (34 μL, 0.25 mmol) was added via syringe. The reaction mixture was heated at 110 °C, and the flask was flushed with compressed air at hourly intervals. After being heated for 24 h, the reaction mixture was cooled to room temperature and filtered through a plug of Celite, and the solvent removed under reduced pressure. Sodium bicarbonate (saturated solution in water) was added to neutralize the residue, and the organic products were extracted into ethyl acetate. The organic extracts were washed with brine, dried over magnesium sulfate, and concentrated in vacuo. ¹H NMR spectroscopic (integration of the CH₂ signal) and gas chromatographic analysis of the crude product was used to calculate conversion ($t_{R1} = 6.53$ min, $t_{R2} = 9.06$ min), and the acetoxylation product **2** was then purified by flash chromatography on silica gel (35% EtOAc in hexane). General Procedure B, acetoxylation of 8-methylquinoline **1** under O₂: To a Schlenk tube fitted with a Young's tap and magnetic stirrer bar were added Pd precatalyst (0.0125 mmol, 5 mol % with respect to substrate) and NaNO₃ (0–1 equiv relative to substrate). The flask was attached to a grease-free Schlenk line fitted with Young's taps and was then evacuated (aspirator vacuum) and backfilled with oxygen three times to achieve 1 atm of O₂. The flask was sealed and heated at 110 °C for 24 h. Reaction workup followed procedure A as described above.

8-Acetoxyethylquinoline **2**, known compound: R_f 0.22 (EtOAc/hexane, 1:3, v/v); ¹H NMR (400 MHz, CDCl₃) δ 8.97 (ddd, $J = 4.2, 1.8, 0.9$ Hz, 1H, H2), 8.19 (dt, $J = 8.3, 1.7$ Hz, 1H, H4), 7.85–7.74 (m, 2H, H5+H7), 7.55 (dd, $J = 8.0, 7.2$ Hz, 1H, H6), 7.45 (ddd, $J = 8.3, 4.2, 0.9$ Hz, 1H, H3), 5.86 (s, 2H, CH₂), 2.16 (s, 3H, CH₃); ¹³C NMR (101 MHz, CDCl₃) δ 171.6 (CO), 150.4 (C2), 146.6 (C9), 136.7 (C4), 134.1 (C8), 129.3 (C6), 128.8 (C7), 126.8 (C5), 124.0 (C10), 121.8 (C3), 63.2 (CH₂), 21.6 (CH₃); HRMS (ESI+) m/z 202.0872 [M + H]⁺ (calcd for C₁₂H₁₂NO₂ 202.0868); IR (ATR, cm⁻¹) 3066, 2925, 1735, 1497, 1365, 1345, 1234, 1065, 1022, 827, 793, 764.

General Protocol for the Kinetics Study of the Complexes in the Acetoxylation Reaction of 1. To a round-bottom flask containing Pd(OAc)₂, **3**, **7a**, **7b**, **8**, or **9** (5 mol %, 0.023 mmol) and NaNO₃ (1 equiv relative to substrate, 39 mg, 0.460 mmol) was added AcOH/Ac₂O (8 mL, 7:1 v/v, air-saturated and preheated at 80 °C). 8-Methylquinoline (1 equiv, 61 μL, 0.460 mmol) was added via syringe. The reaction mixture was heated at 80 °C. Aliquots (0.1 mL) were taken from the reaction mixture every minute during 20 min. Aliquots of the reaction were immediately quenched by addition of 0.5 mL of NH₄Cl saturated solution. The acetoxylation product was then extracted with 0.5 mL of ethyl acetate, filtered through a Pasteur pipet, and filled with cotton wool and Celite into a GC vial containing 1 mL of the mesitylene stock solution (12.4 mmol/L, used as a standard reference for the GC measurements). The GC method consists of three separate washes with three different solvents between each injection. Each sample was injected three times, giving three independent values for each time interval. Individual points, within each kinetic curve, represent the average value of these data (error bars are shown in Figure 10).

Protocol for the Head Space Analysis of the Acetoxylation Reaction Catalyzed by Pd(OAc)₂. In a 500 mL round-bottom flask equipped with a condenser were added Pd(OAc)₂ (25.8 mg, 0.115 mmol, 0.05 equiv), NaNO₃ (195.5 mg, 2.30 mmol, 1 equiv), AcOH/Ac₂O (40 mL, 7:1, v/v), and 8-methylquinoline (305 μL, 2.30 mmol, 1 equiv). Before the mixture was heated at 110 °C, the top of the condenser was equipped with a glass tubing-based piece allowing the entrance of a flux of “zero-air” and the exit to the NO_x detectors. The volume dilution was 15 L per minute, and concentrations are reported in mixing ratios, in this case, in parts per trillion.

General Procedure for the Formation of the Overoxidized Product 10 from Acetoxylation Product 2. To a microwave flask containing Pd(OAc)₂ (0.0181 mmol, 5 mol % relative to **2**) and NaNO₃ (1 equiv relative to **2**) was added 8 mL of AcOH/Ac₂O (7:1).

Compound **2** (73 mg, 0.36 mmol) was added. The reaction mixture was stirred at 110 °C for 24 h, cooled to room temperature, and filtered through a plug of Celite, and the solvent removed under reduced pressure. CH₂Cl₂ was added, and the organic phase was extracted three times with 2 M NaCl (in water). The organic phase was dried over MgSO₄ and filtered and the solvent evaporated under vacuum (to give product **2**). The aqueous phase was acidified with 2 M HCl and extracted three times with ethyl acetate. The organic phase was dried over MgSO₄ and filtered and the solvent removed under vacuum (product **10**). Due to the difficulty associated with the analysis and quantification of the presence of the overoxidized product (to give acid compound **10**), both by MS and GC, the proportion of the acetoxylation and acid products are given in terms of yields following purification (in Figure 13).

■ ASSOCIATED CONTENT**📄 Supporting Information**

The Supporting Information is available free of charge on the ACS Publications website at DOI: 10.1021/jacs.6b10853.

Additional experimental data, full product characterization details (including NMR spectra), X-ray diffraction data, and DFT calculations are supplied (PDF)
X-ray data for complex **3** (CIF)

■ AUTHOR INFORMATION**Corresponding Author**

*ian.fairlamb@york.ac.uk

ORCID

Joshua T. W. Bray: 0000-0003-2384-9675

Ian J. S. Fairlamb: 0000-0002-7555-2761

Present Addresses

[†]School of Chemistry, Cardiff University, Main Building, Park Place, Cardiff CF10 3AT, U.K.

[‡]Thomas Graham Building, University of Strathclyde, 295 Cathedral Street, Glasgow G1 1XL, U.K.

Notes

The authors declare no competing financial interest.

■ ACKNOWLEDGMENTS

The research leading to these results has received funding from the Innovative Medicines Initiative Joint Undertaking under Grant Agreement No. 115360, resources of which are composed of financial contributions from the European Union's Seventh Framework Programme (FP7/2007-2013) and EFPIA companies' in kind contribution (to M.N.W. and I.J.S.F.). We are grateful to the University of York for funding. EPSRC funded the computational equipment used in this study (ref EP/H011455/and EPSRC 'ENERGY' grant, ref no. EP/K031589/1). We appreciate the constructive critical comments provided by the reviewers of our paper.

■ REFERENCES

- (1) (a) *C–H and C–X Bond Functionalization. Transition Metal Mediation*; Ribas, X., Ed.; RSC Catalysis, Series No. 11; Royal Society of Chemistry, 2013. Recent papers in the area of C–H bond functionalization involving Pd catalysts. (b) Fan, J.-H.; Wei, W.-T.; Zhou, M.-B.; Song, R.-J.; Li, J.-H. *Angew. Chem., Int. Ed.* **2014**, *53*, 6650. (c) Wang, L.; Wang, Y.; Liu, C.; Lei, A. *Angew. Chem., Int. Ed.* **2014**, *53*, 5657. (d) Yan, J.-X.; Li, H.; Liu, X.-W.; Shi, J.-L.; Wang, X.; Shi, Z.-J. *Angew. Chem., Int. Ed.* **2014**, *53*, 4945. (e) Park, T.-H.; Hickman, A. J.; Koh, K.; Martin, S.; Wong-Foy, A. G.; Sanford, M. S.; Matzger, A. J. *J. Am. Chem. Soc.* **2011**, *133*, 20138. (f) Zhu, R.; Buchwald, S. L. *Angew. Chem., Int. Ed.* **2012**, *51*, 1926. (g) Zhang, H.; Shi, R.; Gan, P.; Liu, C.; Ding, A.; Wang, Q.; Lei, A. *Angew. Chem., Int.*

- Ed. **2012**, *51*, 5204. (h) Shan, G.; Yang, X.; Ma, L.; Rao, Y. *Angew. Chem., Int. Ed.* **2012**, *51*, 13070. (i) Saget, T.; Cramer, N. *Angew. Chem., Int. Ed.* **2012**, *51*, 12842. (j) Wang, H.; Li, G.; Engle, K. M.; Yu, J.-Q.; Davies, H. M. L. *J. Am. Chem. Soc.* **2013**, *135*, 6774. (k) Sharma, A.; Hartwig, J. F. *J. Am. Chem. Soc.* **2013**, *135*, 17983. (l) Deng, R.; Huang, Y.; Ma, X.; Li, G.; Zhu, R.; Wang, B.; Kang, Y.-B.; Gu, Z. *J. Am. Chem. Soc.* **2014**, *136*, 4472. For recent mechanistic work, see: (m) Ji, Y.; Plata, E. R.; Regens, C. S.; Hay, M.; Schmidt, M.; Razler, T.; Qiu, Y.; Geng, P.; Hsiao, Y.; Rosner, T.; Eastgate, M. D.; Blackmond, D. G. *J. Am. Chem. Soc.* **2015**, *137*, 13272. (n) Smalley, A. P.; Gaunt, M. J. *J. Am. Chem. Soc.* **2015**, *137*, 10632. For recent papers involving other metals, see: (o) Whitaker, D.; Burés, J.; Larrosa, I. *J. Am. Chem. Soc.* **2016**, *138*, 8384. (p) Cambeiro, X. C.; Ahlsten, N.; Larrosa, I. *J. Am. Chem. Soc.* **2015**, *137*, 15636.
- (2) Zultanski, S. L.; Stahl, S. S. *J. Organomet. Chem.* **2015**, 793, 263.
- (3) Stowers, K. J.; Kubota, A.; Sanford, M. S. *Chem. Sci.* **2012**, *3*, 3192.
- (4) (a) Wang, D.; Zavalij, P. Y.; Vedernikov, A. N. *Organometallics* **2013**, *32*, 4882. (b) Zhang, J.; Khaskin, E.; Anderson, N. P.; Zavalij, P. Y.; Vedernikov, A. N. *Chem. Commun.* **2008**, 3625.
- (5) Wickens, Z. K.; Morandi, B.; Grubbs, R. H. *Angew. Chem., Int. Ed.* **2013**, *52*, 11257.
- (6) Li, J.; Grubbs, R. H.; Stoltz, B. M. *Org. Lett.* **2016**, *18*, 5449.
- (7) Lou, S.-J.; Xu, D.-Q.; Xu, Z.-Y. *Angew. Chem., Int. Ed.* **2014**, *53*, 10330.
- (8) (a) Kuznetsova, N. I.; Likholobov, V. A.; Fedotov, M. A.; Yermakov, Y. J. *Chem. Soc., Chem. Commun.* **1982**, 973. For previous work, see: (b) Tamura, M.; Yasui, T. *Chem. Commun.* **1968**, 1209.
- (9) Henry, P. M. *J. Org. Chem.* **1971**, *36*, 1886.
- (10) Andrews, M. A.; Kelly, K. P. *J. Am. Chem. Soc.* **1981**, *103*, 2894.
- (11) Andrews, M. A.; Cheng, C. W. F. *J. Am. Chem. Soc.* **1982**, *104*, 4268.
- (12) Heumann, A.; Chauvet, F.; Waegell, B. *Tetrahedron Lett.* **1982**, *23*, 2767.
- (13) Andrews, M. A.; Chang, T. C. T.; Cheng, C. W. F. *Organometallics* **1985**, *4*, 268.
- (14) Mares, F.; Diamond, S. E.; Regina, F. J.; Solar, J. P. *J. Am. Chem. Soc.* **1985**, *107*, 3545.
- (15) Bäckvall, J.-E.; Heumann, A. *J. Am. Chem. Soc.* **1986**, *108*, 7107.
- (16) (a) Bajwa, S. E.; Storr, T. E.; Hatcher, L. E.; Williams, T. J.; Baumann, C. G.; Whitwood, A. C.; Allan, D. R.; Teat, S. J.; Raithby, P. R.; Fairlamb, I. J. S. *Chem. Sci.* **2012**, *3*, 1656. For a critical review, see: (b) Fairlamb, I. J. S. *Angew. Chem., Int. Ed.* **2015**, *54*, 10415.
- (17) Warren, M. R.; Brayshaw, S. K.; Hatcher, L. E.; Johnson, A. L.; Schiffers, S.; Warren, A. J.; Teat, S. J.; Warren, J. E.; Woodall, C. H.; Raithby, P. R. *Dalton Trans.* **2012**, *41*, 13173.
- (18) For a useful review on the structure of Pd₃(OAc)₆ and its speciation in the presence of water/alcoholic solvents, see: (a) Bedford, R. B.; Bowen, J. G.; Davidson, R. B.; Haddow, M. F.; Seymour-Julen, A. E.; Sparkes, H. A.; Webster, R. L. *Angew. Chem., Int. Ed.* **2015**, *54*, 6591. Also, see two excellent papers about the purity of Pd(OAc)₂: (b) Carole, W. A.; Colacot, T. J. *Chem. - Eur. J.* **2016**, *22*, 7686. Carole, W. A.; Bradley, J.; Sarwar, M.; Colacot, T. J. *Org. Lett.* **2015**, *17*, 5472.
- (19) Ryabov, A. D.; Eliseev, A. V.; Sergeenko, E. S.; Usatov, A. V.; Zakharkin, L. I.; Kalinin, V. N. *Polyhedron* **1989**, *8*, 1485.
- (20) (a) Davies, D. L.; Donald, S. M. A.; Macgregor, S. A. *J. Am. Chem. Soc.* **2005**, *127*, 13754. (b) Lapointe, D.; Fagnou, K. *Chem. Lett.* **2010**, *39*, 1118.
- (21) Yu, S. - Y.; Fujita, M.; Yamaguchi, K. *J. Chem. Soc., Dalton Trans.* **2001**, 3415.
- (22) (a) Nonoyama, M. *Synth. React. Inorg. Met.-Org. Chem.* **1999**, *29*, 119. (b) Nonoyama, M.; Nakajima, K. *Polyhedron* **1998**, *18*, 533.
- (23) Phosphine ligands typically slow down processes involving Pd^{IV} species; see: Sehna, P.; Taylor, R. J. K.; Fairlamb, I. J. S. *Chem. Rev.* **2010**, *110*, 824.
- (24) For a useful review, see: Nair, V.; Panicker, S. B.; Nair, L. G.; George, T. G.; Augustine, A. *Synlett* **2003**, 156.
- (25) It is feasible that the “washing out” of the ¹⁸O label in the presence of pure O₂ might be promoted by Pd–oxo species, i.e., Pd–NO₃ → Pd–O + NO₂, if the process is reversible. Metal–oxo complexes formed from nitrates are known; see: (a) Jiang, J.; Holm, R. H. *Inorg. Chem.* **2005**, *44*, 1068. Pd-oxidase catalysis has been reviewed; see: (b) Stahl, S. S. *Angew. Chem., Int. Ed.* **2004**, *43*, 3400.
- (26) For the lead references, see: (a) Powers, D. C.; Geibel, M. L.; Klein, J. E. M. N.; Ritter, T. *J. Am. Chem. Soc.* **2009**, *131*, 17050. (b) Racowski, J. M.; Dick, A. R.; Sanford, M. S. *J. Am. Chem. Soc.* **2009**, *131*, 10974.
- (27) Davies reported that additional N^CH ligand is required for effective catalytic turnover in cyclometallated systems containing Ir and Rh; see: Boutadla, Y.; Davies, D. L.; Jones, R. C.; Singh, K. *Chem. - Eur. J.* **2011**, *17*, 3438.
- (28) (a) Mason, J.; Larkworthy, L. F.; Moore, E. A. *Chem. Rev.* **2002**, *102*, 913.
- (29) Witanowski, M.; Stefaniak, L.; Webb, G. A. Nitrogen NMR Spectroscopy. In *Annual Reports on NMR Spectroscopy*; Webb, G. A., Ed.; Elsevier, 1981; p 494.
- (30) White, P. B.; Jaworski, J. N.; Fry, C. G.; Dolinar, B. S.; Guzei, I. A.; Stahl, S. S. *J. Am. Chem. Soc.* **2016**, *138*, 4869.
- (31) ESI-MS has been widely used to study catalytic processes involving organometallic species. For example, to examine intermediates from the Heck reaction: (a) Sabino, A. A.; Machado, A. H. L.; Correia, C. R. D.; Eberlin, M. N. *Angew. Chem., Int. Ed.* **2004**, *43*, 2514. In allylic alkylation, see: (b) Markert, C.; Pfaltz, A. *Angew. Chem., Int. Ed.* **2004**, *43*, 2498.
- (32) LIFDI-MS has been used to study transition-metal fluoride complexes: (a) Dransfield, T. A.; Nazir, R.; Perutz, R. N.; Whitwood, A. C. *J. Fluorine Chem.* **2010**, *131*, 1213. (b) Nova, A.; Erhardt, S.; Jasim, N. A.; Perutz, R. N.; Macgregor, S. A.; McGrady, J. E.; Whitwood, A. C. *J. Am. Chem. Soc.* **2008**, *130*, 15499. Mass spectra produced by LIFDI-MS show little or no fragmentation. Recorded ions are normally dominated by molecular radical cations M^{•+}; see: Smith, F. D.; Schaub, M. T.; Rodgers, R. P.; Hendrickson, C. L.; Marshall, A. G. *Anal. Chem.* **2008**, *80*, 7379.
- (33) (a) Baumann, C. G.; De Ornellas, S.; Reeds, J. P.; Storr, T. E.; Williams, T. J.; Fairlamb, I. J. S. *Tetrahedron* **2014**, *70*, 6174–6187. (b) Tang, D.-T. D.; Collins, K.; Glorius, F. *J. Am. Chem. Soc.* **2013**, *135*, 7450–7452.
- (34) *Infrared and Raman Characteristic Group Frequencies, Tables and Charts*, 3rd ed.; Socrates, G., Ed.; John Wiley and Sons Ltd., 2004.
- (35) Jones, C. J.; McCleverty, J. A.; Rothin, A. S.; Adams, H.; Bailey, N. A. *J. Chem. Soc., Dalton Trans.* **1986**, 2055.
- (36) Park, W.; Na, Y.; Baek, D.-J. *Bull. Korean Chem. Soc.* **2006**, *27*, 2023.
- (37) Wah, H. L. K.; Postel, M.; Tomi, F. *Inorg. Chem.* **1989**, *28*, 233.
- (38) Aellig, C.; Girard, C.; Hermans, I. *Angew. Chem., Int. Ed.* **2011**, *50*, 12355.
- (39) Cámpora, J.; Palma, P.; del Río, D.; Carmona, E.; Graiff, C.; Tiripicchio, A. *Organometallics* **2003**, *22*, 3345.
- (40) Haines, B. E.; Berry, J. F.; Yu, J.-Q.; Musaev, D. G. *ACS Catal.* **2016**, *6*, 829.
- (41) (a) Zhang, W.; Ren, S.; Zhang, J.; Liu, Y. *J. Org. Chem.* **2015**, *80*, 5973. Valuable mechanistic and synthetic studies have also been reported recently: (b) Liang, Y.-F.; Li, X.; Wang, X.; Yan, Y.; Feng, P.; Jiao, N. *ACS Catal.* **2015**, *5*, 1956.
- (42) Still, W. C.; Kahn, M.; Mitra, A. *J. Org. Chem.* **1978**, *43*, 2923.
- (43) (a) Csaszar, P.; Pulay, P. *J. Mol. Struct.* **1984**, *114*, 31. (b) Ahlrichs, R.; Bar, M.; Haser, M.; Horn, H.; Kolmel, C. *Chem. Phys. Lett.* **1989**, *162*, 165. (c) Eichkorn, K.; Treutler, O.; Ohm, H.; Haser, M.; Ahlrichs, R. *Chem. Phys. Lett.* **1995**, *240*, 283. (d) Treutler, O.; Ahlrichs, R. *J. Chem. Phys.* **1995**, *102*, 346. (e) Eichkorn, K.; Weigend, F.; Treutler, O.; Ahlrichs, R. *Theor. Chem. Acc.* **1997**, *97*, 119. (f) von Arnim, M.; Ahlrichs, R. *J. Chem. Phys.* **1999**, *111*, 9183. (g) Deglmann, P.; Furche, F. *J. Chem. Phys.* **2002**, *117*, 9535. (h) Deglmann, P.; Furche, F.; Ahlrichs, R. *Chem. Phys. Lett.* **2002**, *362*, 511. (i) Deglmann, P.; May, K.; Furche, F.; Ahlrichs, R. *Chem. Phys. Lett.* **2004**, *384*, 103.